Implications of an integrated late Ediacaran to early Cambrian stratigraphy of the Siberian Platform, Russia

Implications of an integrated late Ediacaran to early Cambrian stratigraphy of the Siberian Platform, Russia

Fred T. Bowyer[1]*, Andrey Yu. Zhuravlev[2], Rachel Wood[1], Fangchen Zhao[3], Sergei S. Sukhov[4], Ruaridh D. Alexander[1], Simon W. Poulton[5], and Maoyan Zhu[3,6]*

[1]School of GeoSciences, University of Edinburgh, James Hutton Road, Edinburgh EH9 3FE, UK.

[2]Department of Biological Evolution, Faculty of Biology, Lomonosov Moscow State University Leninskie Gory 1(12), Moscow 119234, Russia.

[3]State Key Laboratory of Palaeobiology and Stratigraphy, Nanjing Institute of Geology and Palaeontology and Center for Excellence in Life and Palaeoenvironment, Chinese Academy of Sciences, Nanjing 210008, China.

[4]Siberian Scientific Research Institute of Geology, Geophysics and Mineral Resources, Krasny prospect 67, Novosibirsk 630091, Russia.

[5]School of Earth and Environment, University of Leeds, Leeds LS2 9JT, UK.

[6]College of Earth and Planetary Sciences, University of Chinese Academy of Sciences, Beijing 10049, China.

*Corresponding authors: Fred Bowyer (fred.bowyer@ed.ac.uk); Maoyan Zhu (myzhu@nigpas.ac.cn)

ABSTRACT

The transition from the terminal Ediacaran to lower Cambrian (ca. 550–530 Ma) witnessed both the decline of Ediacaran-type soft-bodied and skeletal biota and the rapid diversification of Cambrian-type skeletal biota that dominate the Terreneuvian (ca. 538.8–521 Ma) fossil record. This interval hosts globally widespread positive and negative $\delta^{13}C_{carb}$ excursions, including a negative $\delta^{13}C_{carb}$ excursion near the Ediacaran-Cambrian boundary termed the 1n/BACE. Efforts to produce a global composite chemostratigraphic and biostratigraphic correlation through this interval are complicated by stratigraphic incompleteness and a dearth of radiometric ages to constrain $\delta^{13}C_{carb}$ chemostratigraphy. Extensive and richly fossiliferous open marine carbonates of the Siberian Platform were deposited from the terminal Ediacaran to beyond Cambrian Series 2, and offer a unique archive to refine this chemostratigraphic and biostratigraphic framework. Here we present new $\delta^{13}C_{carb}$ data from two sections of the southeastern Siberian Platform, and synthesize these with published $\delta^{13}C_{carb}$ data from multiple sections throughout the Siberian Platform, that record near-continuous carbonate deposition from the latest Ediacaran to Cambrian Series 2. This allows the construction of two possible chemostratigraphic age models that conform to a coherent framework of lithostratigraphic correlation and platform-wide stratal stacking patterns. These age models are used to test alternative calibrations of fossil first appearances and the spatiotemporal evolution of carbonate deposition on the Siberian Platform. Both models support a pre-1n/BACE appearance of anabaritids in the most distal open-marine sections, and confirm a transitionary Ediacaran-Cambrian biotic assemblage that consists of co-occurring cloudinids and anabaritids. Sedimentological and sequence stratigraphic analysis on the Siberian Platform also provides strong evidence to indicate that the 1n/BACE marks the onset of a gradual, pulsed rise in relative sea level that was sustained throughout the Terreneuvian and Series 2 of the Cambrian.

INTRODUCTION

The last ca. 11 million years of the Ediacaran (ca. 550–538.8 Ma) through to the Fortunian Stage of the Cambrian (ca. 538.8–529 Ma), records the first appearance of skeletal metazoans (ca. 550 Ma), the last appearance of the soft-bodied 'Ediacaran biota' (ca. 538.8–536 Ma), and the first appearance and rapid diversification of small skeletal fossils (SSFs) (Maloof et al., 2010a; Kouchinsky et al., 2017; Zhu et al., 2017; Wood et al., 2019). This interval also hosts an increase in diversity and complexity of mobile trace-making organisms (Cribb et al., 2019), and the first appearance datum (FAD) of the ichnospecies *Treptichnus pedum*, currently used to define the base of the Cambrian Period in the global stratotype section and point (GSSP) at Fortune Head, Newfoundland (Brasier et al., 1994a). A prominent negative $\delta^{13}C_{carb}$ excursion, known as '1n' (e.g. Kouchinsky et al., 2007) or the Basal Cambrian $\delta^{13}C_{carb}$ excursion, the 'BACE' (e.g., Zhu et al., 2006), is also considered to be approximately coincident with the Ediacaran-Cambrian boundary. However, the ages of onset and recovery of the 1n/BACE remain unresolved (Narbonne et al., 1994; Corsetti and Hagadorn, 2000; Zhu et al., 2019; Bowyer et al., 2022).

Attempts to construct Ediacaran to early Cambrian age models have followed a methodological hierarchy whereby high resolution radiometric data (commonly U-Pb geochronology from volcanic tuff interbeds) anchor $\delta^{13}C_{carb}$ in globally distributed marine carbonate deposits (Maloof et al., 2010a; Macdonald et al., 2013; Yang et al., 2021; Bowyer et al., 2022; Nelson et al., 2022). The resulting temporally constrained values of $\delta^{13}C_{carb}$ act as a guide to best-fit high resolution $\delta^{13}C_{carb}$ data from carbonate-dominated successions, and this in turn allows temporal calibration of fossil records in each stratigraphic succession, and between globally-distributed marine environments. The foundations for age model calibration are robust regional chronostratigraphic frameworks that permit confident lateral correlation of

$\delta^{13}C_{carb}$ and paleontological datasets. Despite four decades of targeted research, there is still ambiguity in the local vs global correlation of $\delta^{13}C_{carb}$ across the Ediacaran-Cambrian transition, which obscures evolutionary dynamics throughout this critical interval (reviewed in Bowyer et al., 2022). These uncertainties largely result from a dearth of radiometric data for key sections, in addition to regional differences in stratigraphic continuity and/or lithological suitability, and facies biases for key boundary marker fossils (Babcock et al., 2014).

The highest resolution radiometric data from the Ediacaran-Cambrian boundary interval (ca. 543–538 Ma) anchor $\delta^{13}C_{carb}$ on the Kalahari and Amazonian cratons of Gondwana, in addition to Oman and Laurentia (Grotzinger et al., 1995; Bowring et al., 2007; Parry et al., 2017; Linnemann et al., 2019; Hodgin et al., 2020; Nelson et al., 2022). Crucially, however, each of these successions suffers from an incomplete $\delta^{13}C_{carb}$ record due to significant siliciclastic, evaporitic and/or phosphatic strata, in addition to uncertainties in the duration of non-deposition associated with unconformities and exposure surfaces. The highest resolution $\delta^{13}C_{carb}$ records of the Terreneuvian derive from the Zavkhan terrane, Mongolia (Brasier et al., 1996; Smith et al., 2016a; Topper et al., 2022), the Anti-Atlas, Morocco (Maloof et al., 2005, 2010b), and the Siberian Platform (Brasier et al., 1994b; Kaufman et al., 1996; Pelechaty et al., 1996a, 1996b; Pelechaty, 1998; Kouchinsky et al., 2005, 2007, 2017). Of these, the Zavkhan succession is a promising candidate for resolving Fortunian biostratigraphy, but suffers from difficulties in lateral correlation due to tectonic complexity (Smith et al., 2016a; Topper et al., 2022). By contrast, the Anti-Atlas record has limited Fortunian biostratigraphic control due to a dearth of fossils (Maloof et al., 2010a).

The chemostratigraphic and biostratigraphic potential of Ediacaran-Cambrian successions across the extensive Siberian Platform, Russia, has been recognized for over half a century (e.g. Savitskiy, 1962; Rozanov, 1967). The Siberian Platform formed a separate cratonic

province during the Ediacaran-Cambrian (e.g. Merdith et al., 2021) and hosted a diverse biota representing approximately one third of all known early Cambrian skeletal species (Zhuravlev and Naimark, 2005). However, despite extensive research, the litho-, chemo- and biostratigraphic correlations of sections that may host the regional first appearance of Fortunian SSFs, remain contentious (Zhu et al., 2017; Topper et al., 2022).

Here, we present new $\delta^{13}C_{carb}$ data from two key fossiliferous sections that outcrop along the Yudoma River on the southeast Siberian Platform. This area was targeted as it hosts a thick record of terminal Ediacaran and Terreneuvian open marine strata (Semikhatov et al., 2003; Khomentovsky and Karlova, 2005; Zhu et al., 2017). These new data are first considered in the context of the regional litho-, bio- and chemostratigraphy of the southeastern Siberian Platform. We then synthesise available litho-, bio- and chemostratigraphic information within ten study regions of the Siberian Platform (Fig. 1), to reconstruct two possible composite chemostratigraphic reference curves that are grounded in platform-wide sequences of consistent stratal stacking patterns. Trends in the resulting Siberian $\delta^{13}C_{carb}$ reference curves are then subjected to best-fit visual alignment relative to radiometrically calibrated $\delta^{13}C_{carb}$ values from globally distributed sections. This approach permits a tentative age calibration for Siberian chemostratigraphy and biostratigraphy based on all available data. The resulting composite age models calibrate first occurrences of biota in fifty sections from all ten study regions across the Siberian Platform (Figs. 1, S1–S7). The implications of both possible Siberian age models for global biostratigraphy and the spatiotemporal evolution of carbonate deposition on the Siberian Platform, are considered and discussed.

GEOLOGICAL BACKGROUND OF THE SIBERIAN PLATFORM

Siberian Platform overview

The Siberian Platform consists of several distinct study regions, which form part of an extensive Ediacaran-Cambrian shallow marine platform, with saliniferous-clastic, transitional to open marine carbonate facies belts, the boundaries of which migrated and changed during platform evolution (Figs. 1 and 2). Study regions correspond either with regional tectonic associations (e.g., Igarka-Norilsk Uplift, Anabar Shield, Olenek Uplift) or geographic areas (e.g., Lena River, Yenisei Range, Khara-Ulakh Mountains). Formations within and between each study region have been correlated using lithostratigraphy, biostratigraphy and chemostratigraphy ($\delta^{13}C_{carb}$ and $^{87}Sr/^{86}Sr$) in numerous publications (Figs. S1–S7). The thickest Ediacaran-Cambrian siliciclastic-dominated successions were deposited as molasse in a series of foreland basins that formed during Ediacaran collision of several island arcs and microcontinents with the southwestern margin of the Siberian Craton (Fig. 1, Sovetov, 2002). These foreland basin deposits outcrop in the Yenisei Range, the Irkutsk Amphitheatre, and the Baikal and Patom highlands of southwestern Siberia (study regions I and II of Figs. 1 and 2) (e.g. Pokrovsky, 2006, 2012; Marusin et al., 2021). Boreholes and sections of the platform interior record deposition within a vast saliniferous-clastic facies province, with late Ediacaran to Cambrian deposits that are dominated by interbedded carbonates (dominantly dolostones) and evaporites (study region III of Figs. 1 and 2) (Kochnev et al., 2018). A transitional facies province composed of multiple study regions separated the saliniferous platform interior from deeper open marine facies during the Terreneuvian (study regions IV to IX of Figs. 1 and 2). This transitional facies province is dominated by interbedded dolostones and fossiliferous limestones (e.g. Knoll et al., 1995a,b; Kaufman et al., 1996; Kouchinsky et al., 2007, 2017). Open marine carbonate and outer shelf shale deposits dominated the eastern Siberian Platform

(study regions IX and X of Figs. 1 and 2), and regionally in the Olenek Uplift and Khara-Ulakh Mountains of the northeastern Siberian Platform (study regions VI and VII of Figs. 1 and 2), during the terminal Ediacaran and Terreneuvian.

The southeastern Siberian Platform

The Uchur-Maya study region of southeastern Siberia is the easternmost region of the Yudoma-Anabar facies province, and constitutes the Uchur-Maya Plate to the west and the Yudoma-Maya Belt (Depression) to the east (study regions IX and X of Figs. 1 and 2) (Khomentovsky, 1986). The boundary between these two structural units is defined along strike of the Nel'kan-Kyllakh thrust fault complex (Khomentovsky and Karlova, 2002; Khomentovsky, 2008). In the Uchur-Maya study region, mixed siliciclastic and carbonate deposits of the Aim and Ust'-Yudoma formations of the Ediacaran Yudoma (Sardana) Group onlap an inherited paleorelief composed of various units that are interpreted as pre-Ediacaran in age, of which the youngest is the Cryogenian Ust'-Kirbi Formation (Uy Group) (Khomentovsky, 1986).

Fossiliferous sections of the Uchur-Maya Plate exposed along the banks of the Aldan River and tributaries to the south have been historically important for the definition of Siberian regional stage subdivision of the Cambrian. In this regard, two of the most important sections, Dvortsy and Ulakhan-Sulugur, were some of the first Terreneuvian sections to undergo systematic and integrated bed-scale lithostratigraphic and paleontological description, and geochemical sampling for $\delta^{13}C_{carb}$ (Magaritz et al., 1986; Brasier et al., 1993). This resulted in some of the first Cambrian records of litho- and chemostratigraphically calibrated biostratigraphy (Brasier et al., 1993). The Aim Formation is not present at Dvortsy; here dolostone of the Ust'-Yudoma Formation nonconformably overlies an inherited paleorelief of crystalline basement. Small skeletal fossils of anabaritids and chancelloriids first occur in Bed

8 of the upper Ust'-Yudoma Formation at Dvortsy, following recovery from a negative $\delta^{13}C_{carb}$ excursion which is thought to correspond with the 1n/BACE (Brasier et al., 1993).

The Ust'-Yudoma Formation thickens to the east, where it overlies dark and often sulfurous limestones of the upper Aim Formation (Khomentovsky, 2008). Along the Yudoma River near the Kyra-Ytyga River mouth, high resolution $\delta^{13}C_{carb}$ data have been used to infer a pre-1n/BACE age for the Ust'-Yudoma Formation (Zhu et al., 2017). This observation was based on the consistency of trends and magnitudes of $\delta^{13}C_{carb}$ between this section and the pre-1n/BACE upper Dengying Formation of the Yangtze Platform, South China, as well as western Laurentia and various other radiometrically-calibrated late Ediacaran successions (Zhu et al., 2017; Bowyer et al., 2022). The biostratigraphic implications of a pre-1n/BACE correlation for the fossiliferous upper unit at the Kyra-Ytyga section, which results in a very early first occurrence of SSFs of the *Purella antiqua* assemblage Zone relative to other global occurrences, is controversial (Topper et al., 2022). A detailed assessment of the possible correlations for this section, and resulting implications for global biostratigraphy, are discussed herein.

METHODS

Stratigraphic logging and geochemical sampling

Sampling was undertaken along the Yudoma River, Republic of Sakha (Yakutia), Russia. Fieldwork along the Yudoma River was concentrated at three thick, continuous, and very well exposed key sections, for which the lithostratigraphy and paleontology have been systematically described in the published literature (e.g. Semikhatov et al., 2003; Khomentovsky and Karlova, 2005). Sampled sections are located at the Yudoma-Maya

confluence (YM), Nuuchchalakh valley (NV), and Kyra-Ytyga River mouth (KY) (Figs. 3 and S7). These study sections constitute individual cliff exposures along the banks of the Yudoma River. At each section, sedimentary logging, and paleontological and geochemical sampling were carried out systematically, following a single transect from the base to the top of each section, with sampling heights determined through use of a folding meter stick. Geochemical samples (~25 g) were collected at 0.5–1 m resolution, where possible.

Carbonate $\delta^{13}C$ chemostratigraphy

Samples from YM and NV were microdrilled from individual laminations where possible, or from the finest microcrystalline material. Veins, fractures and siliciclastic components were not sampled, with the exception of some dolomite-cemented siliciclastics from the Aim Formation at NV section, which are separately indicated in the figures and in Table S1. The resulting powders were analyzed for their carbonate carbon and oxygen isotopic composition at the Nanjing Institute of Geology and Palaeontology, and an additional sample set from NV was analyzed at the University of Edinburgh Wolfson Laboratory. All isotopic ratios are reported in per mil notation relative to the composition of the Vienna Pee Dee Belemnite (VPDB). Replicate analyses of standards yielded standard deviations (1σ) of better than ±0.08‰ for $\delta^{13}C$ and better than ±0.12‰ for $\delta^{18}O$. Full details of all analytical procedures are provided in the supplementary material. Carbon isotope chemostratigraphy of the KY section has previously been reported by Zhu et al. (2017), and is shown herein for lateral section correlation and comparison.

Composite carbon isotope age model construction by visual alignment

All available published lithostratigraphic, biostratigraphic and $\delta^{13}C_{carb}$ chemostratigraphic information for each study region of the Siberian Platform has been synthesized to create a series of stratigraphic correlation charts for fifty sections (Figs. S1–S7). Detailed bed-by-bed litho- and biostratigraphic information has been translated from original Russian publications to reconstruct some sections of the southeast Siberian Platform (Fig. S7 and supplementary material). We use the resulting correlation charts to inform the most parsimonious lithostratigraphic and chemostratigraphic correlations within and between each region. In most instances, section correlations are consistent with those proposed in previous studies (e.g. Anabar and Olenek uplifts, Pelechaty et al., 1996b, 1996a; Kouchinsky et al., 2017), and resulting $\delta^{13}C_{carb}$ peak correlations are labelled individually (Figs. S2–S7). Next, we compare the lithostratigraphy, biostratigraphy, chemostratigraphy and stratal stacking patterns between study regions, and explore the implications of alternative correlations to create two composite $\delta^{13}C_{carb}$ reference curves for the Siberian Platform that are consistent with all available data. Differences between these reference curves are associated with ongoing uncertainties in section correlations (labelled in Figs. S2–S7).

In order to visualize and temporally calibrate trends in the resulting composite $\delta^{13}C_{carb}$ reference curves, we adopt a procedure of visual $\delta^{13}C_{carb}$ alignment following the methods outlined in Bowyer et al. (2022). Each individual section is subdivided into units of continuous lithology and interpreted facies (e.g. shallow marine oolitic limestone, outer shelf to slope shale), with depositional rates that are assumed to be continuous throughout. Different depositional rates between units are consistent with the lithology and facies within each unit, and the differences in depositional rates between units permits flexibility in $\delta^{13}C_{carb}$ peak alignment. Temporal hiatuses are permitted at surfaces of erosion or exposure. Gaps in the

carbon isotope record are also permitted within significant intervals of siliciclastic deposition for which $\delta^{13}C_{carb}$ data are not available. Lastly, we use the scaffold of available radiometrically calibrated $\delta^{13}C_{carb}$ data for the terminal Ediacaran and lower Cambrian updated from Model C of Bowyer et al. (2022) with new data from the Nama Group of South Africa (Nelson et al., 2022), to create a visual best-fit temporal calibration for the Siberian $\delta^{13}C_{carb}$ reference curves. This approach allows calibration of associated fossil occurrences directly within chemostratigraphic age models.

A shortcoming of the visual alignment methodology is an inability to quantitatively define uncertainties for age ranges of fossil first occurrences in intervals that are not radiometrically well constrained. A more quantitative approach to chemostratigraphic correlation has been attempted between three lower Cambrian sections of Morocco that benefit from very high resolution and continuous $\delta^{13}C_{carb}$ datasets (Hay et al., 2019). However, a pre-requisite to reliable interpretations of computed chemostratigraphic alignment is to accurately account for uncertainties in lithostratigraphic correlation. Our synthesis presents $\delta^{13}C_{carb}$ correlations for fifty sections that are considerably variable in their stratigraphic completeness, and in the resolution of published $\delta^{13}C_{carb}$ datasets (Figs. S2–S7). These sections also occupy a variety of distinct study regions, and facies-related preservation and/or diagenesis may result in differences in the fidelity of preservation of primary seawater $\delta^{13}C_{carb}$ within and between regions (discussed further below). These limitations demand that biostratigraphic and chemostratigraphic correlations be carefully considered section by section within a framework of all possible lithostratigraphic correlations. In our contribution, we synthesize the necessary prerequisite stratigraphic information for the Siberian Platform that, we hope, may aid future quantitative alignments using dynamic programming algorithms.

RESULTS

Lithostratigraphy and paleontology of the Yudoma River sections

Detailed bed-by-bed lithostratigraphic and sedimentological descriptions for each section are provided in the supplementary material, and summarized below.

The YM section outcrops near the confluence with the Maya River (YM, Figs. 3C, 4A–C, S7). Here, the section is composed of 34 m of dolostones, minor siltstones and sandstones of the Aim Formation, followed by >130 m of coarse sandy dolostone and dolomite-cemented sandstone with lenticular dolostone beds or nodules of the Ust'-Yudoma Formation (Wood et al., 2017b). Ediacaran-age soft-bodied fossils are relatively abundant in sandstones of the Aim Formation, and include *Palaeopascichnus* chambered fossils and *Aspidella*-type frondomorph holdfasts, in addition to abundant *Beltanelliformis* (Ivantsov, 2017, 2018; Wood et al., 2017a, 2017b; Zhu et al., 2017), of which the latter may represent colonial cyanobacteria (Bobrovskiy et al., 2018). Dolomitic packstones of the Aim Formation immediately above the *Aspidella*-bearing interval also host *Suvorovella aldanica*, thought to be a dolomtized analogue of *Aspidella* (Vologdin and Maslov, 1960; Ivantsov, 2017; Wood et al., 2017a, 2017b; Zhu et al., 2017) (Fig. 4C). The *Suvorovella*-bearing unit is laterally extensive to over 1 km and contains broken shell fragments and microbial oncoids, with a prominent karstic surface near the top. This unit is followed by a 13.5 m-thick cross-laminated dolomudstone overlain by trough-laminated medium-grained quartzose sandstone, the top of which has been taken as the boundary between the Aim and Ust'-Yudoma formations at this section (Wood et al., 2017a) (Fig. 3C).

The NV section is located approximately 80 km up-river from YM (Figs. 3D, 4D, S7). At NV, the Aim Formation is subdivided into two members. The lower member is 65.6 m thick

and composed of a succession of sandstone, shale, dolomudstone and dolomitic packstone (Fig. 4E, F). The overlying member is approximately 31 m thick, and composed of a thin basal unit (max. 1.0 m) of glauconitic dolostone, sandstone, and dolomitic breccia with ooids and dolomitic stromatolites, followed by siltstone, dolomite-cemented siltstone, dolomudstone and subordinate stromatolitic and thrombolitic carbonate (Fig. 4E, G). The uppermost 1–2 m of the Aim Formation is composed of black, organic-rich dolomitic limestone. Dolomite-cemented mudstone in the second member of the Aim Formation at NV contain abundant *Nenoxites* on bedding surfaces (previously assigned to *Gaojiashania*; Zhuravlev et al., 2009), and various acritarch species (Pyatiletov, 1988; Zhu et al., 2017). *Nenoxites* is also present in an overlying unit of dark, laminated stromatolitic and thrombolitic limestone. A sharp, undulose surface marks the boundary between the upper Aim Formation and light grey shallow marine dolostone of the lower Ust'-Yudoma Formation (Fig. 4H). The lower Ust'-Yudoma Formation hosts a prominent, laterally discontinuous unit that contains angular to sub-angular clasts of silty dolostone with darker laminae (Fig. 4I). The clast composition appears similar to a unit of laminated dolostone within the lower Ust'-Yudoma Formation (Fig. 4J), which implies that the clast-bearing interval represents an intraformational breccia. The darker, ribbon-like laminae in this interval may represent microbial mats or hardgrounds (Fig. 4J). Overlying this unit, the Ust'-Yudoma Formation contains wavy laminated dolomudstone, with darker laminae that may represent microbial mat fabrics and synsedimentary cavities infilled by early fibrous and radial dolomite cement. The uppermost 15 m of the Ust'-Yudoma Formation at NV is composed of finely alternating white to yellowish-grey, wavy-laminated dolomudstone and oolitic grainstone, with occasional ~10 cm-long wackestone lenses that contain the first occurrence of the SSF *Anabarites trisulcatus* in this section. The contact between the Ust'-Yudoma Formation and overlying Tommotian variegated limestones of the Pestrotsvet Formation is not exposed at NV.

306 The KY section outcrops near the Kyra-Ytyga River mouth on the Yudoma River, ~70 km
307 up-river from NV and approximately 50 km down river from the remote township of
308 Yugorenok (Figs. 3B,E, 5A, S7). At KY, the Aim Formation rests disconformably upon an
309 inherited paleorelief composed of conglomeratic to coarse sandstones of the Ust'-Kirbi
310 Formation (Fig. 5B) and, as at NV, sediments of the Aim Formation can be subdivided into
311 two members. The lower Aim Formation constitutes a succession of unfossiliferous cross-
312 bedded grey sandstones with red shale interbeds, and an overlying unit of light and dark grey
313 dolomudstone with visible pyrite. The upper Aim Formation is composed of dark, laminated
314 limestones with organic carbon-rich black calcareous shale interbeds containing soft-bodied
315 fossils, including *Nenoxites* (=*Shaanxilithes*) and *Beltanelliformis* (Zhu et al., 2017) (Fig. 5C).
316 A sharp contact separates the upper Aim Formation at KY from overlying prograding shallow
317 marine dolostones of the Ust'-Yudoma Formation (Fig. 5D). Limestones of the upper Aim
318 Formation at KY yield a carbonate Pb-Pb isochron age of 553 ± 23 Ma (2σ, MSWD = 0.8),
319 and $^{87}Sr/^{86}Sr$ values (mean = 0.70839, n = 7) that are consistent with least altered $^{87}Sr/^{86}Sr$ data
320 from globally distributed sections in the interval ca. 549–528 Ma (Semikhatov et al., 2003;
321 Bowyer et al., 2022).

322 Dolostones of the lower Ust'-Yudoma Formation transition to mixed dolomitic limestones
323 and an upper unit of parallel laminated limestone and dolomitic limestone (Zhu et al., 2017).
324 Skeletal fossils appear in the uppermost Ust'-Yudoma Formation at KY within limestones and
325 dolomitic limestones, including the terminal Ediacaran *Cloudina* and *Anabarites* (Figs. 3E and
326 6) (Zhu et al., 2017). A rich skeletal assemblage including protoconodonts and anabaritids,
327 together with large orthothecimorph hyoliths and the trace fossil *Diplocraterion*, appear in the
328 uppermost 8 m of light-grey dolomitic limestone of the Ust'-Yudoma Formation at KY (Figs.
329 3E and 6) (Zhu et al., 2017). Some of these SSFs are representative of the *Purella antiqua*
330 Zone, which has classically been regarded as upper Nemakit-Daldynian in age, based on

occurrences in strata to the south of the Aldan River and in sections of the Anabar Shield on the northern Siberian Platform (Figs. 3E, 6, S1 and S4) (Kaufman et al., 1996; Kouchinsky et al., 2017). The Pestrotsvet Formation has not been reported at this section (Khomentovsky, 2008; Wood et al., 2017b; Zhu et al., 2017).

Sequence stratigraphic interpretation of the Yudoma River sections

The three studied sections are interpreted to record a shelf-edge transect across the south-eastern margin of the Siberian Platform, with the shallowest facies recording a proximal depositional setting on the Uchur-Maya Plate (YM), to increasingly distal settings towards the northeast at NV and in the Yudoma-Maya Depression (KY) (Figs. 1 and 3) (Wood et al., 2017b). Each sequence is composed of transgressive systems tracts represented by dolomite-cemented siltstones and shales (YM and NV) or laminated limestone (KY), followed by highstand systems tracts of shallow marine dolostones, with various fabrics that are inferred to be of microbial origin. Dolostone therefore dominates these successions, except in the late transgressive systems tract of the Aim Formation, and in the uppermost ~10–70 m of the Ust'-Yudoma Formation (Fig. 3).

We interpret the Aim Formation to represent at least one and a half cycles of accommodation change. The lower member of the Aim Formation corresponds to one full sequence (Sequence 1), with transgressive onlap of the inherited paleorelief represented by a succession of lithologies of increasing depth. The maximum flooding surface of this sequence is interpreted to correlate with the fossiliferous siltstone interval at YM and the acritarch-bearing shale interval at NV. Subsequent regression and shallowing during the overlying highstand systems tract is recorded by the *Suvorovella* shell bed at YM and dark grey dolostones at the top of the

lower Aim Formation at NV and KY. This highstand systems tract is capped by a karstic surface at YM. Mixed dolomite-cemented siltstones and dark red (ferruginous) shales at NV, and dark laminated limestones and organic-rich shales at KY, which constitute the second member of the Aim Formation, were deposited during a series of shallowing upward parasequences of the subsequent transgression (Sequence 2, Figs. 3D and 4E,F). At NV, the uppermost red shale unit has been interpreted to represent the maximum flooding surface, and is subsequently overlain by dolomite-cemented siltstone with green shale interbeds (Wood et al., 2017b).

The contact between the Aim and Ust'-Yudoma formations is undulose at NV, and sharp at KY (Figs. 4H, 5D). It is unclear whether this surface represents a sequence boundary, or a condensed interval near the maximum flooding surface in the upper Aim Formation. As such, the upper Aim Formation can be interpreted to represent either one full cycle of accommodation change with an erosive contact at a sequence boundary, or one half cycle, with the maximum flooding surface separating the Aim and Ust'-Yudoma formations. These alternative interpretations have significant implications for litho-, chemo- and biostratigraphic correlation of the Ust'-Yudoma Formation.

Carbon isotope chemostratigraphy of the Yudoma River sections

All new $\delta^{13}C_{carb}$ data from YM and NV sections are provided in Table S1. In Sequence 1 of the lower Aim Formation at YM, there is a smooth decrease in $\delta^{13}C_{carb}$, from high values in shallow marine transgressive dolostones (max = 2.75‰), through mixed sandstone, siltstone and micritic dolomite of the fossiliferous maximum flooding surface, to lower values in highstand systems tract dolomitic *Suvorovella* shell hash (Fig. 3C). Values reach a nadir of -

0.84‰ in shallow marine dolostones of Sequence 2, which overlie the karstic surface capping the *Suvorovella* bed that marks the top of Sequence 1 at this locality (Fig. 3C).

Highstand dolostones in Sequence 1 of the Aim Formation at NV show a gradual decreasing trend from 1‰ to a nadir of -1.22‰. Dolomite-cemented siltstones and minor dolostone interbeds that were deposited during transgression comprise the subsequent fossiliferous upper Aim Formation, and record a smooth recovery to positive $\delta^{13}C_{carb}$ values that stabilize ~0.80‰ (Fig. 3D). In the final 10–15 m of the carbonate-dominated upper Aim Formation, $\delta^{13}C_{carb}$ values remain positive (~0.60‰), with minor negative values (min = -0.49‰) that correspond with a lithological transition from silty dolostone to a thin dolomite-cemented siltstone interbed. Dolomite samples of the lowermost Ust'-Yudoma Formation record positive $\delta^{13}C_{carb}$ (max = 2.26‰) with a minor negative excursion to -0.39‰ at ~125 m, followed by stable positive values (max = 2.17‰). A prominent negative $\delta^{13}C_{carb}$ excursion with a nadir of -3.59‰ is recorded at ~185 m, and is accompanied by negligible change in $\delta^{18}O$ (Fig. 3D). The recovery to positive values at ~205 m is followed by a stable plateau around a mean value of 1.6‰ throughout the following ~75 m, prior to a decline to ~0‰ recorded by dolostones near the top of the section.

$\delta^{13}C_{carb}$ chemostratigraphy of the KY section has been reported by Zhu et al. (2017), and data are shown in Fig. 3E. Here, dolostones deposited during the highstand systems tract of the lower Aim Formation record decreasing $\delta^{13}C_{carb}$ from 1.61‰ to -0.75‰ immediately beneath the sequence boundary. The upper Aim Formation records positive $\delta^{13}C_{carb}$, with two peaks that reach a maximum of 3.95‰ prior to a gradual decline in the upper limestone interval of the formation. $\delta^{13}C_{carb}$ values reach a nadir of -1.27‰ at the top of the Aim Formation. Samples from the overlying Ust'-Yudoma Formation show a rising trend from scattered values near the formation boundary, to reach a peak of 3.18‰ in the lower Ust'-Yudoma Formation. The onset

401 of gradually decreasing $\delta^{13}C_{carb}$, which begins at ~164 m, is not accompanied by any notable
402 change in dominant lithology or facies. The decreasing $\delta^{13}C_{carb}$ trend in the upper Ust'-Yudoma
403 Formation at KY culminates in a nadir of -0.65‰ in laminated fossiliferous limestones at the
404 top of the section.

405 Data from samples of the Yudoma River occupy the same space in cross-plots of $\delta^{13}C_{carb}$
406 and $\delta^{18}O$ as the majority of sections in the compiled Siberian Platform dataset (Fig. 7A).
407 Samples of dolomite and mixed dolomitic limestone of the Ust'-Yudoma Formation at NV and
408 KY share a similar range in $\delta^{18}O$ (Fig. 7B, C). Samples of dolomite from the Aim Formation
409 at YM, NV and KY also share a similar range in $\delta^{18}O$ (Fig. 7D–F). However, dolomite samples
410 of the upper Aim Formation at YM and NV have elevated $\delta^{18}O$ relative to limestones of the
411 upper Aim Formation at KY (Fig. 7D–F). Here, samples of dolomite and dolomite-cemented
412 siltstone at YM and NV are characterised by a wider range (0.60 to -8.44‰) and isotopically
413 heavier mean $\delta^{18}O$ (-2.68‰) than limestones of the Aim Formation at KY, which occupy a
414 narrow range of $\delta^{18}O$ (-5.44‰ to -8.09‰) with a lighter mean composition (-6.55‰).

415

416 **DISCUSSION**

417 **Dolomitization and lateral carbon isotopic gradients in seawater**

418 Regional and global $\delta^{13}C_{carb}$ correlations rely on the assumption that carbonate minerals
419 faithfully preserve the carbon isotopic composition of open marine dissolved inorganic carbon
420 (DIC) during crystal growth and throughout subsequent diagenesis (Veizer and Hoefs, 1976;
421 Kaufman et al., 1991; Halverson et al., 2010; Maloof et al., 2010a). Such correlations also rely
422 on the assumption that the average isotopic composition of open marine DIC is globally
423 homogeneous on early diagenetic timescales, with long-term changes that are dominated by

the global export/burial rates of inorganic and organic carbon (Keith and Weber, 1964; Veizer and Hoefs, 1976; Veizer et al., 1980; Kaufman et al., 1991). However, there are several instances where these assumptions may be challenged. The $\delta^{13}C_{carb}$ composition of carbonate sediments may be decoupled from the isotopic composition of open marine DIC via diurnal coupling of photosynthesis and carbonate saturation in shallow seawater (Geyman and Maloof, 2019), facies restriction and local pools of DIC with isotopic compositions distinct from open seawater (Melim et al., 2002; Cui et al., 2020), and sediment-buffered versus fluid-buffered diagenetic regimes (Ahm et al., 2019; Hoffman and Lamothe, 2019; Bold et al., 2020; Nelson et al., 2021). Of these processes, facies restriction and different diagenetic regimes are likely the most problematic for high-resolution regional $\delta^{13}C_{carb}$ chemostratigraphy. The degree to which these factors affect the utility of open marine carbonates to archive long-term global trends in seawater $\delta^{13}C$ is less clear. Radiometrically calibrated $\delta^{13}C_{carb}$ age models appear to support the synchroneity of numerous Neoproterozoic $\delta^{13}C_{carb}$ excursions (Macdonald et al., 2013; Yang et al., 2021; Bowyer et al., 2022), but variability in the magnitude of these excursions within and between regions may be controlled to some degree by sediment-buffered versus fluid-buffered diagenetic regimes (Ahm et al., 2019, 2021). Any such effects will necessarily be more problematic when attempting to calibrate intervals of geologic time that are characterised by muted carbon cycle variability. Furthermore, a dearth of radiometric ages currently precludes unequivocal correlation of $\delta^{13}C_{carb}$ throughout the Fortunian to Stage 3 of the Cambrian.

Dolostone dominates Ediacaran and Fortunian successions of the SE Siberian Platform. Along the Yudoma River, several observations lead to the conclusion that pervasive dolomitization was very early, and also very rapid (Wood et al., 2017b). First, siltstone to dolomite transitions occur laterally over mm to m scales in the upper Aim Formation at NV, and breccias in the siltstone horizons contain clasts that show various degrees of

449 dolomitization, suggesting early replacement (Wood et al., 2017b). Second, many fabrics in
450 dolostones that occupy highstand systems tracts are composed of homogeneous
451 microcrystalline dolomite. In very shallow dolograinstones that occur just below the middle
452 Aim Formation sequence boundary at YM, grains and *Suvovovella* molds are preserved as
453 intact micrite envelopes that show no features of collapse or compaction, and are encrusted by
454 isopachous dolomite crusts (Wood et al., 2017b). Organic-walled acritarchs are also preserved
455 within encrustations of microcrystalline dolomite in the lower Aim Formation at NV (Wood et
456 al., 2017b). Lastly, primary cavities in dolostones of the Aim and the Ust'-Yudoma formations
457 are lined with radial dolomite cements of length-slow character, similar to marine dolomite
458 cements reported from the Cryogenian interglacial Umberatana Group (Hood and Wallace,
459 2012; Wood et al., 2017b). These dolomite cements are iron-rich and zoned, and their
460 formation is interpreted to have been promoted under anoxic water column conditions (Wood
461 et al., 2017b). The interpretation of early dolomite cementation of the siltstones may also be
462 corroborated by the $\delta^{13}C_{carb}$ data presented herein from dolomite-cemented siltstone samples
463 of the upper Aim Formation at NV (Fig. 3D). These samples record a gradual smooth recovery
464 from a minor negative $\delta^{13}C_{carb}$ excursion recorded in dolomudstones of the underlying
465 highstand systems tract, and this recovery is recorded in laterally equivalent shallow marine
466 dolostone at YM (Figs. 3C, D). However, $\delta^{13}C_{carb}$ recorded by primary marine dolomite may
467 be affected, to varying degree, by sediment-buffered versus fluid-buffered diagenesis (e.g.,
468 Ahm et al., 2019), and the degree to which this early dolomite records the composition of
469 contemporaneous seawater therefore remains uncertain.$\delta^{18}O$ increases with progressive
470 shallowing towards the middle Aim Formation sequence boundary at both YM and NV, before
471 decreasing through the upper Aim Formation at NV (Fig. 3C, D), which may reflect changes
472 in the degree of dolomitization. $\delta^{13}C_{carb}$ data from the second member of the Aim Formation

also show consistent trends between dolomite at YM and NV that appear to be distinct from the trends recorded in limestone of the same interval at KY.

We explore two possible mechanisms to explain the observed differences in $\delta^{13}C_{carb}$ data between these three sections. The first is that the distinct patterns of $\delta^{13}C_{carb}$ recorded in the upper Aim Formation result from partial facies restriction and/or dolomitization at YM and NV relative to KY. The second is that there is a temporal hiatus at the boundary between the Aim and Ust'-Yudoma formations at NV, correlative with ongoing deeper marine deposition at KY. In order to investigate the possibility for a stratigraphic hiatus at the Aim/Ust'-Yudoma Formation boundary, we explore the lateral lithostratigraphic correlation of sections that outcrop across the Uchur-Maya Plate.

Stratigraphic correlation of the southeastern Siberian Platform

The fossiliferous late Ediacaran to Cambrian Aim and Ust'-Yudoma formations of the southeastern Siberian Platform were the focus of intense stratigraphic and paleontological scrutiny by Russian scientists from the early 1980s to 2000s (Khomentovsky et al., 1983, 1990; Val'kov, 1983; Val'kov and Karlova, 1984; Khomentovsky and Karlova, 1986, 1989, 1991, 1993; Khomentovsky, 2008). With the exception of some overview papers (Khomentovsky and Karlova, 1993, 2002, 2005; Khomentovsky, 2008), the majority of the resulting original Russian publications have not been translated into English, and the lithostratigraphic and biostratigraphic details for many sections have therefore remained largely underappreciated by the wider scientific community. Here we provide detailed bed-by-bed descriptions and fossil occurrence information for nine key fossiliferous sections of the Uchur-Maya Plate that outcrop along river banks and cliffs to the south of the Aldan River, in the vicinity of the Uchur, Gonam,

Aim and Maya rivers. We use these descriptions to construct a lithostratigraphic correlation chart with associated fossil occurrence information (Figs. 8, S7). The lithostratigraphic and biostratigraphic details, which include direct translations from original Russian publications, are provided in the supplementary material. We caution that, despite every attempt to reproduce these sections at the highest resolution possible, sections 1 to 9 each represent composite profiles of the Ust'-Yudoma Formation that are not easily correlated between one another (Fig. 8). As a result, even the original authors interpret their own data differently in successive publications. For example, Figure 4 of Khomentovsky & Karlova (2005) indicates, at Mt Konus (section 5) and Nemnekey River (section 6), a single level with fauna of the *Purella antiqua* Zone, and this indication contradicts their previous publications, which we use here, and their own Tables 1 and 2, which document fossils in the same paper. As such, precise levels of fossil occurrences within each section, and the lateral correlation of individual members between sections, remain tentative.

Despite the associated uncertainties, several key observations are possible. Firstly, documented occurrences of small skeletal fossils are largely restricted to intervals of (often thinly bedded) limestone or dolomitic limestone, where fossils are better preserved (consistent with the observations of Kouchinsky et al., 2017). Secondly, the first occurrences of anabaritids, protoconodonts and chancelloriids pre-date the first occurrences of halkieriids, hyoliths, hyolithelminthes and mollusks in almost all successions where several SSF levels are reported. Thirdly, the boundary between the Aim and Ust'-Yudoma formations has been described as erosional in two additional sections to the south of the Aldan River (sections 2 and 3, Fig. 8).

At Dvortsy, anabaritids and chancelloriids first occur in Bed 8 of the upper Ust'-Yudoma Formation. However, it is widely accepted that the lower extent of the *Purella antiqua* SSF

Zone should correspond with the base of member 3 after lateral correlation to Mt Konus (section 5, Fig. 8) (Brasier et al., 1993). This pattern of fossil occurrence, whilst consistent with the first observation of preservational bias, requires verification due to the difficulty in robust lateral correlation of the boundary between members 2 and 3. Brasier et al. (1993) provided three $\delta^{13}C_{carb}$ measurements from the Mt Konus-Nemnekey River region, the results of which appear consistent with the historical member subdivision. However, robust chemostratigraphic calibration of fossil occurrences in the Ust'-Yudoma Formation at Mt Konus and Nemnekey River demands future studies that integrate paleontological collections and high resolution $\delta^{13}C_{carb}$ in the same sections.

Age models A–D of Bowyer et al. (2022) correlated $\delta^{13}C_{carb}$ trends in the Ust'-Yudoma Formation along the Yudoma River at KY with globally consistent trends in terminal Ediacaran (pre-1n/BACE) strata, after the observations of Zhu et al. (2017). Here, we explore two possible depositional models for the Yudoma River sections that integrate observations of lithostratigraphic correlation from across the Uchur-Maya Plate and Yudoma-Maya Belt. The chemostratigraphic age models that result from these two depositional models differ from age models A–D reported by Bowyer et al. (2022), and so they are distinguished herein as models E and F. Points of evidence in support of, and against, each model are provided below, and the implications of each model for chemostratigraphy and biostratigraphy are subsequently discussed.

Model E assumes that there is no hiatus at the boundary between the Aim and Ust'-Yudoma formations at KY, and possibly also at NV (Fig. 9A–C). In this model, limestones of the upper Aim Formation along the Yudoma River, and in the deeper sections to the south of the Aldan River, were deposited during a single transgression across the Uchur-Maya Plate and Yudoma-Maya Belt (Fig. 9A). The observed differences in $\delta^{13}C_{carb}$ between NV and KY during this

interval may correspond with facies restriction at NV, or lateral differences in the isotopic composition of DIC, whereby possible methanogenesis within the anoxic and organic carbon-rich deep waters promoted the retention of isotopically heavy $\delta^{13}C_{carb}$ in finely laminated (microbial mat) limestones. Alternatively, these differences may reflect variability in the preservation of seawater $\delta^{13}C_{carb}$ associated with sediment-buffered versus fluid-buffered diagenesis of primary marine carbonates (e.g., Ahm et al., 2019).

The ribbon dolomite of the lower Ust'-Yudoma Formation at NV may represent hemipelagic deposition, consistent with the depositional interpretation for ribbon limestone described from the Waterton Formation of the Mesoproterozoic Belt Supergroup (Pratt and Rule, 2021). Prograding dolostone sequences of the Ust'-Yudoma Formation were subsequently deposited during a highstand systems tract (Fig. 9B). In this model, the undulose surfaces at the boundary between the Aim and Ust'-Yudoma formations at NV and at sections 2 and 3 (Fig. 8) are interpreted to represent soft-sediment loading by prograding dolostone sequences. In both models E and F, the inferred basin paleobathymetry, which deepened towards the east, permits the earlier onset of dolomite deposition of the Ust'-Yudoma Formation at NV, and allows the negative $\delta^{13}C_{carb}$ excursion in the middle Ust'-Yudoma Formation at NV to correlate with the negative trend in data at the boundary between the Aim and Ust'-Yudoma formations at KY. The greater accommodation space in the deeper setting at KY also permits a greater thickness of dolostone to accumulate during progradation. In Model E, the entire Ust'-Yudoma Formation at NV and KY is interpreted as a lateral equivalent to member 1 and lower member 2 of sections to the west, after the historical lithostratigraphic subdivision (Fig. 8). Finally, the uppermost units of laminated limestone and dolomitic limestone at NV and KY are interpreted to correspond with transgression that resulted in onlap of the crystalline basement to the west at Dvortsy, the lower half of which is reassigned to

member 2 (Fig. 9C). This model results in a pre-1n/BACE correlation for the entire Ust'-Yudoma Formation at NV and KY, consistent with the interpretation of Zhu et al. (2017).

Model F assumes that the boundary between the Aim and Ust'-Yudoma formations represents a sequence boundary with a variable extent of erosion between sections, and a possible significant hiatus in deposition (Fig. 9D). In Model F, the onset of the 1n/BACE occurred during deposition of the upper Aim Formation, which was subsequently lost to erosion. Transgression across the Uchur-Maya Plate then led to onlap of the crystalline basement at Dvortsy (Fig. 9E), and prograding sequences of the overlying highstand captured the recovery from the 1n/BACE at Dvortsy, and led to the successive deposition of prograding sequences from west to east across the Uchur-Maya Plate and Yudoma-Maya Belt (Fig. 9F). Model F therefore leads to a post-1n/BACE correlation for the sections at NV and KY, whereby the best-fit visual alignment would correlate positive $\delta^{13}C_{carb}$ in the lower Ust'-Yudoma Formation at NV with an expanded lateral equivalent to interval 'Z' at Dvortsy (Fig. 8). The upper Ust'-Yudoma Formation at NV and the entire Ust'-Yudoma Formation at KY would then correspond with peak 'I' at Dvortsy (Fig. 8). One potentially serious problem with Model F is that, given the current understanding of paleobathymetry between Dvortsy, YM, NV and KY, this model requires a prolonged interval of non-deposition at NV and KY, for which there is no observable evidence in the field.

A third possible depositional model, which would not require an unconformable boundary between the Aim and Ust'-Yudoma formations, would assume that transgressive onlap of the basement at Dvortsy occurred coincident with deposition of the upper Aim Formation. In this model, lateral differences in $\delta^{13}C_{carb}$ between sections of the Aim Formation are attributable to facies restriction, dolomitization, or lateral differences in the isotopic composition of DIC, similar to the assumptions made in Model E. This model would result in a post-1n/BACE

correlation for the upper Ust'-Yudoma Formation fossil assemblage recorded at KY, similar to Model F. However, both this model and Model F result in a peculiar absence of mollusks from the uppermost fossiliferous beds at NV and KY when considering the historical correlation of members of the Ust'-Yudoma Formation (Fig. 8). Furthermore, both this model and Model F necessarily result in a very late occurrence of *Cloudina* at KY relative to all other global sections (discussed below).

Integrated stratigraphic correlation of the Siberian Platform

Previous studies integrating late Ediacaran $\delta^{13}C_{carb}$ chemostratigraphy and sequence stratigraphy across the Siberian Platform have correlated section information from the Anabar Shield, Olenek Uplift, Khara-Ulakh Mountains, Aldan River, and Baikal and Patom highlands (Figs. 1, S1–S7) (Knoll et al., 1995a, 1995b; Kaufman et al., 1996; Pelechaty et al., 1996a, 1996b; Pelechaty, 1998; Cui et al., 2016). In their correlation framework, Pelechaty et al. (1996a) documented secular trends in $\delta^{13}C_{carb}$ that were represented in multiple sections of the northeastern Siberian Platform, which they used to reconstruct the regional evolution of basin geometry. These Ediacaran strata were subdivided into three major depositional sequences (S1 to S3) on the basis of chemo- and sequence stratigraphy (Figs. 10, S5) (Pelechaty et al., 1996a). Despite regional distinction in tectonic and depositional settings, facies, and geographic separation, this correlation framework was subsequently applied to a section on the opposing side of the Siberian Platform >1000 km to the south (Nokhtuysk, Figs. 11, S2) (Pelechaty, 1998). In brief, the resulting composite $\delta^{13}C_{carb}$ profile shows peak values nearing 5‰ in upper Sequence 1, followed by a short-lived negative excursion in Sequence 2 and a recovery to positive values in Sequence 3. Values of $\delta^{13}C_{carb}$ decline to ~0‰ in Sequence 3, followed by an interval of relatively invariant $\delta^{13}C_{carb}$ in the region of 0–1‰, and a final downturn to

616 negative $\delta^{13}C_{carb}$ in the Turkut Formation, immediately below a karst surface at the top of
617 Sequence 3 (Pelechaty et al., 1996b; Pelechaty, 1998) (Fig. 10). The base of the Turkut
618 Formation may record the regional FAD of the anabaritid *Cambrotubulus* (Rogov et al., 2015)
619 (Fig. 10), which defines the base of the regional Nemakit-Daldynian Stage, and the downturn
620 in $\delta^{13}C_{carb}$ recorded immediately below the upper karst surface is classically interpreted to
621 correspond with the onset of the 1n/BACE.

622 The Khatyspyt Formation displays broad trends in $\delta^{13}C_{carb}$ and lithostratigraphy that
623 correspond well with the Aim Formation along the Yudoma River (Fig. 11). This is especially
624 the case at KY, where thinly laminated limestones of the upper Aim Formation record values
625 of $\delta^{13}C_{carb}$ of up to 3.95‰ (Figs. 3, 8 and 10). In Model E, the Aim and Ust'-Yudoma
626 formations along the Yudoma River are conformable, and were deposited approximately
627 contemporaneously with the Khatyspyt and Turkut formations of the Olenek Uplift. This is
628 consistent both with previous assessments (Khomentovsky, 2008), and with the presence of
629 Ediacaran soft-bodied fossils in the lower formations and skeletal fauna of the *Anabarites*
630 *trisulcatus* Zone in the overlying ones.

631 A maximum age for intrusion of the Tas-Yuryakh volcanic breccia of the lower Syhargalakh
632 Formation along the Khorbusuonka River is suggested by a zircon U-Pb air abrasion ID-TIMS
633 age of 542.8 ± 1.30 Ma (Bowring et al., 1993; Maloof et al., 2010a; Rogov et al., 2015). The
634 Tas-Yuryakh volcanic breccia unconformably overlies the Turkut Formation (Fig. 10), thereby
635 providing an estimated maximum age for the top of the Turkut Formation. It is anticipated that
636 redating of the Tas-Yuryakh volcanic breccia using updated zircon preparation and analytical
637 techniques for U-Pb geochronology, will result in a refined age interpretation for the top of the
638 Turkut Formation (discussed further in Bowyer et al., 2022). To date, the karst surface reported
639 from the Turkut Formation and equivalent units of the Khara-Ulakh Mountains has not been

correlated to the Ust'-Yudoma Formation along the Yudoma River. In Model E, this may be explained by more continuous deposition of the Ust'-Yudoma Formation in southeast Siberia (Khomentovsky, 2008). This interpretation may also be consistent with an inferred genesis of the karst surface in the Olenek Uplift linked to regional uplift of the northern and eastern margins of the platform (Kiselev et al., 2018). By contrast, Model F may imply that the karst surface at the top of Sequence 3 is equivalent either to the sequence boundary in the middle of the Aim Formation, or the contact between the Aim and Ust'-Yudoma formations along the Yudoma River.

Carbonate conglomerates of the Tinnaya Formation in the Nokhtuysk section of the Baikal and Patom highlands (Figs. 1, 11, S2) display predominantly negative $\delta^{13}C_{carb}$ immediately above a karst surface (Pelechaty, 1998). Pelechaty (1998) considered trends in $\delta^{13}C_{carb}$ recorded in the Tinnaya Formation to correlate with their sequences 2 and 3. At the time of publication of these studies, no fossils had been reported from the Nokhtuysk section to guide a more accurate biostratigraphic and chemostratigraphic correlation. However, more recent paleontological studies report *Cambrotubulus* sp. and chancelloriid sclerites from 52 m below the top of the Tinnaya Formation, and *Cambrotubulus* sp., *Anabarites trisulcatus* and *Tiksitheca* sp. at a level 14 m below the top of the Tinnaya Formation at Nokhtuysk (Fig. 11) (Khomentovsky et al., 2004; Mel'nikov et al., 2005). In light of these biostratigraphic reports, and greater ease of $\delta^{13}C_{carb}$ correlation, we tentatively consider the karst surface at the base of the Tinnaya Formation to correspond with the karst surface at the top of the Turkut Formation (Figs. 10 and 11). However, we note that $\delta^{13}C_{carb}$ and $\delta^{18}O_{carb}$ values of the Nokhtuysk section are distinct from all other sections of the Siberian Platform (Fig. 7A), which may cast some doubt on confident chemostratigraphic alignments (Pelechaty, 1998). In this revised correlation, the carbonate conglomerates of the Tinnaya Formation were deposited during onlap associated with platform-wide drowning, which remains consistent

665 with the original suggestion of Pelechaty (1998), with minor realignment to Sequence 4. This
666 correlation maintains consistent trends in $\delta^{13}C_{carb}$ associated with the '0n' and '1n' negative
667 $\delta^{13}C_{carb}$ excursions in the Izluchina and Sukharikha formations of the Sukharikha River section
668 (Kouchinsky et al., 2007), the Ust'-Yudoma Formation at Dvortsy along the Aldan River
669 (Magaritz et al., 1986; Brasier et al., 1993), and possibly the Staraya Rechka Formation of the
670 Kotuykan River (Knoll et al., 1995b; Kaufman et al., 1996) (Fig. 11).

671 The onset of the 1n/BACE marks a shift in long-term global $\delta^{13}C_{carb}$ trends that distinguish
672 the late Ediacaran from Fortunian Stage carbon isotopic records. Whilst the late Ediacaran
673 (<550 Ma) is characterised by generally positive $\delta^{13}C_{carb}$ interrupted by short-lived negative
674 $\delta^{13}C_{carb}$ excursions, the Fortunian Stage is dominated by negative $\delta^{13}C_{carb}$, interrupted by short-
675 lived positive $\delta^{13}C_{carb}$ excursions (Kouchinsky et al., 2007; Maloof et al., 2010a; Smith et al.,
676 2016a). Fossiliferous carbonate successions from across the Siberian Platform that were
677 deposited during Sequence 4 show a pattern of $\delta^{13}C_{carb}$ consistent with the global Fortunian
678 record (Fig. 11). This pattern is documented in both dolostone (e.g. Sukharikha, Dvortsy, Fig.
679 11) and limestone (e.g. Kotuykan, Kugda and Ary-Mas-Yuryakh, Figs. 11 and S4) sections,
680 which suggests that $\delta^{13}C_{carb}$ correlation is not significantly impeded by dolomitization in this
681 interval (Kouchinsky et al., 2017). However, variable section completeness results in ongoing
682 uncertainties in peak correlation within and between study regions. In Model E, we follow the
683 correlation of Kouchinsky et al. (2017) by correlating peak 5p at Sukharikha with the positive
684 $\delta^{13}C_{carb}$ excursion recorded in the Medvezhya Formation at Kotuykan, and peak 'I' at Dvortsy
685 (Figs. 11, S4). However, in Model F, we correlate the positive excursions in the Medvezhya
686 Formation at Kotuykan, Kugda and Ary-Mas-Yuryakh, and all peaks in the lower Emyaksin
687 Formation at Bol'shaya Kuonamka, with peak 6p at Sukharikha (Fig. S4). These alternative
688 correlations result in significantly different patterns of platform-wide sequence correlation and
689 succession completeness (Fig. 12A, B).

690

691 **Calibrating the Siberian composite $\delta^{13}C_{carb}$ reference curve**

692 Uncertainty remains in the temporal position of the 1n/BACE onset (reviewed in Bowyer et
693 al., 2022). The highest precision radiometric data available from volcanic ash deposits that are
694 interbedded within successions that host terminal Ediacaran soft-bodied and skeletal fossils
695 derive from the Nama Group of Namibia and South Africa, where the 1n/BACE has not been
696 recorded (Linnemann et al., 2019; Nelson et al., 2022). If carbonates in the Nama Group
697 succession record the isotopic composition of global seawater, one possible stratigraphic
698 correlation follows that the onset of the 1n/BACE post-dates the youngest radiometric
699 constraint derived from the Nama Group, and is therefore younger than ~538 Ma (Saylor et al.,
700 1998; Linnemann et al., 2019; Bowyer et al., 2022; Nelson et al., 2022). This inferred age for
701 the 1n/BACE onset is consistent with models C and D of Bowyer et al. (2022).

702 Our age models E and F assume continuous deposition of the Mastakh, Khatyspyt and
703 Turkut formations along the Khorbusuonka River (Fig. 10). The best-fit visual alignment of
704 these data with the radiometrically calibrated $\delta^{13}C_{carb}$ scaffold (updated after Model C of
705 Bowyer et al., 2022) suggests that deposition of the lower Turkut Formation commenced
706 approximately contemporaneously with the upper Urusis and lower Nomtsas formations of the
707 Nama Group (Fig. 12A, B). The subsequent Fortunian Stage currently lacks radiometric ages
708 to anchor high frequency shifts in $\delta^{13}C_{carb}$, resulting in significant uncertainty in
709 chemostratigraphic calibration. However, an unpublished age of 529.7 ± 0.3 Ma tentatively
710 anchors peak $\delta^{13}C_{carb}$ values that are assumed to correlate with 5p in the Mattaia Formation of
711 the Olenek Uplift (Kaufman et al., 2012), and peaks 6p and Atdabanian peak IV are
712 radiometrically well constrained in Morocco (Maloof et al., 2010b; Landing et al., 2020). The
713 Cambrian Stage 2 to 4 interval benefits from a continuous high resolution $\delta^{13}C_{carb}$ reference

curve derived from limestones of the Lena River, which calibrates distinct SSF, archaeocyath and trilobite assemblage zones (Fig. S6) (Brasier et al., 1994b). As such, the reduction in scatter of the $\delta^{13}C_{carb}$ reference curve from stages 2 to 4 may result from both the dominantly limestone lithology in this interval, in addition to greater confidence in $\delta^{13}C_{carb}$ alignments that are corroborated by robust biozonation.

In both models E and F, pre-1n/BACE open marine deposition on the Siberian Platform was restricted to the peripheral northeastern and southeastern (present orientation) study regions (Fig. 12C). The onset of the 1n/BACE occurred near a major sequence boundary (Fig. 12A, B). Overall, this broad pattern of chemostratigraphy and stratal stacking patterns is notably similar to the pre-1n/BACE record of the Mackenzie and Wernecke mountains of northwestern Canada, the Zavkhan Terrane of Mongolia, and the Yangtze Platform of South China (Zhu et al., 2007; Macdonald et al., 2013; Smith et al., 2016a). Transgressive onlap during the lower Fortunian Stage is suggested by the onset of open marine carbonate deposition in study regions surrounding the western and northern peripheries of the platform, and sections closer to the centre of the platform in both models E and F (Fig. 12D). Subsequent major transgression at the onset of Sequence 5 has long been recognised (Zhuravlev, 1998), and corresponds with deposition of the Pestrotsvet Formation and all correlative (commonly variegated red and green) limestone deposits across the Siberian Platform (Fig. 12A,B,E). This pattern of pulsed lower Cambrian sea level rise on the Siberian Platform correlates with onset of the Sauk transgression of Laurentia, and with historical observations of widespread lower Cambrian relative sea level rise on multiple cratons (Matthews and Cowie, 1979; McKie, 1993; Maloof et al., 2010a).

Implications of Siberian stratigraphic correlation for Ediacaran-Cambrian global biostratigraphy

The base of the Terreneuvian Series and Fortunian Stage of the Cambrian are defined by the FAD of *Treptichnus pedum* at the base of Member 2 of the Chapel Island Formation at Fortune Head, Newfoundland (Brasier et al., 1994a). As with all other fossil occurrences noted below, the presence/absence of this fossil suffers from issues of preservational bias, and the present record clearly remains incomplete. In the current version of the International Chronostratigraphic Chart (2022), an age of 538.8 ± 0.2 Ma is suggested for the Ediacaran-Cambrian boundary, which is based on a radiometric age from a laterally discontinuous ash bed in the lower Nomtsas Formation of the Nama Group, Namibia, in a section that does not host *T. pedum* or the 1n/BACE (Linnemann et al., 2019, 1 in Fig. 13A). More recent biostratigraphic and chemostratigraphic investigation and radiometric dating of the Nama Group in South Africa confirm the absence of *T. pedum* from even younger strata that also do not record the 1n/BACE (Nelson et al., 2022). If the 1n/BACE represents a global perturbation to seawater $\delta^{13}C_{carb}$, and if carbonates of the Nama succession record the composition of open marine $\delta^{13}C_{carb}$, then the most parsimonious conclusion employing all available chemostratigraphic, radiometric and biostratigraphic data follows that the $\delta^{13}C_{carb}$ record of the Nama succession is older than the onset of the 1n/BACE (Models C and D of Bowyer et al., 2022). In all successions that host both *T. pedum* and the 1n/BACE (e.g., Mount Dunfee section of Nevada, Caborca sections of northwestern Mexico, sections of the Zavkhan terrane of Mongolia), the FAD of this ichnospecies occupies a position above the 1n/BACE nadir, no earlier than peak 2p based on visual alignment of $\delta^{13}C_{carb}$ data (3 in Fig. 13A) (Smith et al., 2016a, 2016b; Hodgin et al., 2020; Bowyer et al., 2022). The 1n/BACE (2 in Fig. 13A) is therefore lower Cambrian in age according to the radiometric constraint adopted in the International Chronostratigraphic Chart (2022) (1 in Fig. 13A), or terminal Ediacaran in age

based on its occurrence relative to the FAD of the defining ichnospecies *T. pedum* (3 in Fig. 13A). This distinction is important when considering the ages of regional Siberian stages relative to internationally recognized Cambrian Period subdivision.

The base of the regional Nemakit-Daldynian Stage of Siberia is set at the base of the *Anabarites trisulcatus* Zone containing anabaritids, protoconodonts (*Protohertzina*) and rarely chancelloriids (Khomentovsky and Karlova, 1992, 2005). Based on published biostratigraphy and $\delta^{13}C_{carb}$ chemostratigraphy, the lower boundaries of the *Anabarites trisulcatus* Zone and subsequent *Purella antiqua* Zone [= *P. cristata* Zone], in which orthothecimorph hyoliths, hyolithelminthes, halkieriids and mollusks appeared, have previously been considered correlative with a lower Fortunian, and an upper Fortunian age, respectively (e.g. Kouchinsky et al., 2017). According to both models E and F, the pre-1n/BACE regional first occurrence of *Cambrotubulus* in the lower Turkut Formation of the Olenek Uplift (Fig. 10), which is thought to represent the morphologically-simplest anabaritid, occupies a best-fit visual alignment with the terminal Ediacaran $\delta^{13}C_{carb}$ record by definition of the position of the FAD of *T. pedum* relative to the 1n/BACE (3 in Fig. 13A, Fig. 13B,C). This is in agreement with a possible pre-1n/BACE first appearance of anabaritids in South China, and also with the recently calibrated first appearance of protoconodonts within the 1n/BACE interval in the Zavkhan Terrane of Mongolia (Cai et al., 2019; Topper et al., 2022). The base of the Nemakit-Daldynian regional Stage can therefore be considered uppermost Ediacaran in age until *T. pedum* is reported from strata that confidently predate peak 2p.

Model E results in a pre-1n/BACE correlation for the fossiliferous level at the top of the KY section (Fig. 13B), as originally proposed by Zhu et al. (2017). As stated by Topper et al. (2022), this correlation results in a very early first occurrence of halkieriids, chancelloriids, hyolithelminthes and hyoliths on the southeastern Siberian Platform relative to all other areas.

Despite uncertainties in lateral lithostratigraphic correlation across the Uchur-Maya Plate, this depositional model satisfies field observations reported from KY. By contrast, Model F correlates the uppermost fossiliferous level at KY with peak 5p based on best-fit visual alignment with the Fortunian $\delta^{13}C_{carb}$ record (Fig. 13C). Thus, models E and F have very different implications for the range extension of cloudinids into the Fortunian Stage (Fig. 13D). The cloudinid *Zuunia chimidtsereni* is confirmed in strata of the Zavkhan Terrane, Mongolia, from below the 1n/BACE nadir in the Zuun-Arts Formation, and continues up to the level of peak 2p in the lower Bayangol Formation (Topper et al., 2022). Cloudinids at KY include a specimen confidently assigned to *Cloudina*, with a calcareous tube consisting of nested funnel-like segments, which are not observed in any typical Cambrian SSFs (Fig. 6). In Model E, cloudinids at KY occupy the pre-1n/BACE interval during a time in which *Cloudina* dominates the global skeletal fossil assemblage. By contrast, the best-fit visual alignment of Model F results in a very late occurrence of cloudinids at KY, within the late Fortunian (Fig. 13D).

Importantly, despite ongoing uncertainties in stratigraphic correlation, both models confirm a transitional biotic assemblage across the upper Ediacaran to Fortunian interval. Classic 'Ediacaran' (e.g. cloudinid) and Fortunian (e.g. anabaritid) skeletal fossils co-existed in the Ust'-Yudoma Formation at KY, and the FAD of anabaritids is pre-1n/BACE on multiple cratons. At a minimum (Model F), this transitional assemblage constitutes SSFs of the *Anabarites trisulcatus-Protohertzina anabarica* assemblage Zone alongside cloudinids in carbonate-dominated settings, and typical Ediacaran soft-bodied fossils and cloudinids in mixed siliciclastic-carbonate settings prior to the first documented occurrence of *T. pedum*.

CONCLUSIONS

New data are presented from key late Ediacaran fossiliferous sections of southeastern Siberia. These sections are first correlated regionally using all available published lithostratigraphic information. Two possible depositional models for these strata are then considered relative to published litho-, bio- and chemostratigraphy from other regions of the Siberian Platform that document terminal Ediacaran to Fortunian deposition. The differences between these models relate to ongoing uncertainties in chemostratigraphic alignment that are related to stratigraphic incompleteness or ambiguity in $\delta^{13}C_{carb}$ peak correlation. Exploring both possible models allows the resulting biostratigraphic implications to be clearly visualised, and informs the construction of two possible composite $\delta^{13}C_{carb}$ reference curves for the Siberian Platform that are consistent with major platform-wide stratal stacking patterns and associated sequence stratigraphy. This approach reveals the spatiotemporal evolution of carbonate deposition and patterns of first occurrence of biota across the Siberian Platform throughout the late Ediacaran to Cambrian Series 2.

The Siberian reference curves are calibrated by best-fit visual $\delta^{13}C_{carb}$ alignment with available global radiometrically calibrated $\delta^{13}C_{carb}$ data, permitting tentative chronostratigraphic frameworks for the late Ediacaran and early Cambrian of the Siberian Platform. This integrated approach confirms an early (pre-1n/BACE) appearance of anabaritids in the most distal, open marine sections to the east. Expanding this correlation framework to consider paleontological and $\delta^{13}C_{carb}$ chemostratigraphic records from globally distributed regions reveals a temporal overlap between small skeletal fossils previously interpreted as definitively Cambrian in age, and skeletal and soft-bodied fossils that characterise the terminal Ediacaran fossil record. The absolute duration and extent of this overlap remains unclear due to a dearth of Fortunian radiometric ages and uncertainty in the age of recovery from the

1n/BACE. This biostratigraphic implication is common to both age models considered herein, and inconsistent with a significant global mass extinction event coincident with the 1n/BACE. Instead, it supports a gradual transition between Ediacaran and Cambrian biotic assemblages and a deep root for the Cambrian explosion.

ACKNOWLEDGEMENTS

Funding: FB, RW, SWP and MZ acknowledge funding from the joint NERC-NSFC Biosphere Evolution Transitions and Resilience (BETR) programme (NE/P013643/1, NSFC/41661134048), MZ from the Strategic Priority Research Program (B) of the Chinese Academy of Sciences (XDB 26000000) and National Natural Science Foundation of China (no. 41921002), FB and SWP from NERC project NE/R010129/1, and RW, SWP and FB from NERC Project NE/T008458/1. We thank C. Chilcott for technical support. FB thanks Artem Kouchinsky and Victor Podkovyrov for enlightening discussions. We thank associate editor Brian Pratt and two anonymous reviewers for detailed and thoughtful comments that greatly improved the paper. **Author contributions**: MZ and FB conceived the project, FB compiled all data with the help of AZ, RW and MZ. FB constructed the age model. MZ, FZ, RW, AZ and SS collected Siberian samples. MZ, FZ, RW and RA analyzed Siberian samples. All authors contributed to writing the paper. **Competing interests**: Authors declare no competing interests; **Data and materials availability**: All new data are available in the supplementary material. Full global age models E and F are available upon request.

REFERENCES CITED

Ahm, A.-S.C., Maloof, A.C., Macdonald, F.A., Hoffman, P.F., Bjerrum, C.J., Bold, U., Rose, C.V., Strauss, J.V., Higgins, J.A., 2019, An early diagenetic deglacial origin for basal Ediacaran "cap dolostones": Earth and Planetary Science Letters, v. 506, p. 292–307.

Ahm, A.-S.C., Bjerrum, C.J., Hoffman, P.F., Macdonald, F.A., Maloof, A.C., Rose, C.V., Strauss, J.V., and Higgins, J.A., 2021, The Ca and Mg isotope record of the Cryogenian Trezona carbon isotope excursion: Earth and Planetary Science Letters, v. 568, p. 117002.

Astashkin, V.A., Pegel', T.V., Repina, L.N., Rozanov, A.Yu., Shabanov, Yu.Ya., Zhuravlev, A.Yu., Sukhov, S.S., and Sundukov, V.M., 1991, The Cambrian System on the Siberian Platform. Correlation chart and explanatory notes: International Union of Geological Sciences Publication, no. 27, p. 1–133.

Babcock, L.E., Peng, S., Zhu, M., Xiao, S., and Ahlberg, P., 2014, Proposed reassessment of the Cambrian GSSP: Journal of African Earth Sciences, v. 98, p. 3–10.

Bobrovskiy, I., Hope, J.M., Krasnova, A., Ivantsov, A., and Brocks, J.J., 2018, Molecular fossils from organically preserved Ediacara biota reveal cyanobacterial origin for *Beltanelliformis*: Nature Ecology and Evolution, v. 2, p. 437–440.

Bold, U., Ahm, A.-S.C., Schrag, D.P., Higgins, J.A., Jamsran, E., and Macdonald, F.A., 2020, Effect of dolomitization on isotopic records from Neoproterozoic carbonates in southwestern Mongolia: Precambrian Research, v. 350, p. 105902.

Bowring, S.A., Grotzinger, J.P., Isachsen, C.E., Knoll, A.H., Pelechaty, S.M., and Kolosov, P., 1993, Calibrating rates of Early Cambrian evolution: Science, v. 261, p. 1293–1298.

Bowring, S.A., Grotzinger, J.P., Condon, D.J., Ramezani, J., Newall, M.J., and Allen, P.A., 2007, Geochronologic constraints on the chronostratigraphic framework of the Neoproterozoic Huqf Supergroup, Sultanate of Oman: American Journal of Science, v. 307, p. 1097–1145.

878 Bowyer, F.T., Zhuravlev, A.Y., Wood, R., Shields, G.A., Curtis, A., Poulton, S.W., Condon, D.J., Yang, C.,
879 and Zhu, M., 2022, Calibrating the temporal and spatial dynamics of the Ediacaran-Cambrian
880 radiation of animals: Earth-Science Reviews, 225, p. 103913.

881 Brasier, M.D., Khomentovsky, V.V., and Corfield, R.M., 1993, Stable isotopic calibration of the
882 earliest skeletal fossil assemblages in eastern Siberia (Precambrian-Cambrian boundary): Terra
883 Nova, v. 5, p. 225–232.

884 Brasier, M., Cowie, J., and Taylor, M., 1994a, Decision on the Precambrian-Cambrian boundary
885 stratotype: Episodes, v. 17, p. 3–8.

886 Brasier, M.D., Rozanov, A.Y., Zhuravlev, A.Y., Corfield, R.M., and Derry, L.A., 1994b, A carbon isotope
887 reference scale for the Lower Cambrian Series in Siberia (Report of IGCP Project 303):
888 Geological Magazine, v. 131, p. 767–783.

889 Brasier, M.D., Shields, G., Kuleshov, V.N., and Zhegallo, E.A., 1996, Integrated chemo- and
890 biostratigraphic calibration of early animal evolution: Neoproterozoic–early Cambrian of
891 southwest Mongolia: Geological Magazine, v. 133, p. 445–485.

892 Cai, Y., Xiao, S., Li, G., and Hua, H., 2019, Diverse biomineralizing animals in the terminal Ediacaran
893 Period herald the Cambrian explosion: Geology, v. 47, p. 380–384.

894 Corsetti, F.A., and Hagadorn, J.W., 2000, Precambrian-Cambrian transition: Death Valley, United
895 States: Geology, v. 28, p. 299–302.

896 Cribb, A.T., Kenchington, C.G., Koester, B., Gibson, B.M., Boag, T.H., Racicot, R.A., Mocke, H.,
897 Laflamme, M., and Darroch, S.A.F., 2019, Increase in metazoan ecosystem engineering prior to
898 the Ediacaran–Cambrian boundary in the Nama Group, Namibia: Royal Society Open Science, v.
899 6, p. 190548.

900 Cui, H., Grazhdankin, D.V., Xiao, S., Peek, S., Rogov, V.I., Bykova, N.V., Sievers, N.E., Liu, X.M., and
901 Kaufman, A.J., 2016, Redox-dependent distribution of early macro-organisms: Evidence from

902 the terminal Ediacaran Khatyspyt Formation in Arctic Siberia: Palaeogeography,
903 Palaeoclimatology, Palaeoecology, v. 461, p. 122–139.

904 Cui, H., Warren, L.V., Uhlein, G.J., Okubo, J., Liu, X.M., Plummer, R.E., Baele, J., Goderis, S., Claeys, P.,
905 and Li, F., 2020, Global or regional? Constraining the origins of the middle Bambuí carbon cycle
906 anomaly in Brazil: Precambrian Research, v. 348, p. 105861.

907 Geyman, E.C., and Maloof, A.C., 2019, A diurnal carbon cycle engine explains ^{13}C-enriched
908 carbonates without increasing the global production of oxygen: Proceedings of the National
909 Academy of Sciences of the United States of America, v. 116, p. 24433–24439.

910 Grotzinger, J.P., Bowring, S.A., Saylor, B.Z., and Kaufman, A.J., 1995, Biostratigraphic and
911 geochronological constraints on early animal evolution: Science, v. 13, p. 229–272.

912 Halverson, G.P., Wade, B.P., Hurtgen, M.T., and Barovich, K.M., 2010, Neoproterozoic
913 chemostratigraphy: Precambrian Research, v. 182, p. 337–350.

914 Hay, C.C., Creveling, J.R., Hagen, C.J., Maloof, A.C., and Huybers, P., 2019, A library of early Cambrian
915 chemostratigraphic correlations from a reproducible algorithm: Geology, v. 47, p. 457–460.

916 Hodgin, E.B., Nelson, L.L., Wall, C.J., Barrón-Díaz, A.J., Webb, L.C., Schmitz, M.D., Fike, D.A.,
917 Hagadorn, J.W., and Smith, E.F., 2020, A link between rift-related volcanism and end-Ediacaran
918 extinction? Integrated chemostratigraphy, biostratigraphy, and U-Pb geochronology from
919 Sonora, Mexico: Geology, v. 49, p. 115–119.

920 Hoffman, P.F., and Lamothe, K.G., 2019, Seawater-buffered diagenesis, destruction of carbon
921 isotope excursions, and the composition of DIC in Neoproterozoic oceans: Proceedings of the
922 National Academy of Sciences of the United States of America, v. 116, p. 18874–18879.

923 Hood, A. van S., and Wallace, M.W., 2012, Synsedimentary diagenesis in a Cryogenian reef complex:
924 Ubiquitous marine dolomite precipitation: Sedimentary Geology, v. 255–256, p. 56–71.

925 Ivantsov, A.Y., 2017, Finds of Ediacaran-type fossils in Vendian deposits of the Yudoma Group,
926 Eastern Siberia: Doklady Earth Sciences, v. 472, p. 143–146.

927 Ivantsov, A.Y., 2018, Vendian macrofossils of the Yudoma Group, Southeast of the Siberian Platform:
928 Paleontological Journal, v. 52, p. 1335–1346.

929 Kaufman, A.J., Hayes, J.M., Knoll, A.H., and Germs, G.J.B., 1991, Isotopic compositions of carbonates
930 and organic carbon from upper Proterozoic successions in Namibia: stratigraphic variation and
931 the effects of diagenesis and metamorphism: Precambrian Research, v. 49, p. 301–327.

932 Kaufman, A.J., Knoll, A.H., Semikhatov, M.A., Grotzinger, J.P., Jacobsen, J.P., and Adams, W., 1996,
933 Integrated chronostratigraphy of Proterozoic-Cambrian beds in the western Anabar region,
934 northern Siberia: Geological Magazine, v. 133, p. 509–533.

935 Kaufman, A.J., Peek, S., Martin, A.J., Cui, H., Grazhdankin, D., Rogov, V., Xiao, S., Buchwaldt, R., and
936 Bowring, S., 2012, A shorter fuse for the Cambrian explosion?: Geological Society of America
937 Abstracts with Programs, v. 44, p. 326.

938 Keith, M.L., and Weber, J.N., 1964, Carbon and oxygen isotopic compositions of selected limestones
939 and fossils: Geochimica et Cosmochimica Acta, v. 28, p. 1787–1816.

940 Khomentovsky, V.V., 1985, The Vendian of the Siberian Platform, *in* Sokolov, B.S., and Fedonkin,
941 M.A., eds., Vendskaya sistema, Istoriko-geologicheskoe i paleontologicheskoe obosnovanie, t.
942 2, Stratigrafiya i geologicheskie protsesy: Moscow, Nauka (translated in The Vendian System, v.
943 2, Regional Geology: Berlin; Heidelberg, Springer, 1990), p. 83–161.

944 Khomentovsky, V.V., 1986, The Vendian System of Siberia and a standard stratigraphic scale:
945 Geological Magazine, v. 123, p. 333–348.

946 Khomentovsky, V.V., 2008, The Yudomian of Siberia, Vendian and Ediacaran systems of the
947 international stratigraphic scale: Stratigraphy and Geological Correlation, v. 16, p. 581–598.

948 Khomentovsky, V.V., and Karlova, G.A., 1986, On the lower boundary of the Pestrotsvet Formation in
949 the r. Aldan basin, *in* Khomentovsky, V.V. ed., Late Precambrian and Early Palaeozoic of Siberia,
950 Siberian Platform and the Outer Belt of the Altay-Sayan Foldbelt: Novosibirsk, Insitut Geologii i
951 Geofiziki, Sibirskoe Otdelenie, Akademiya Nauk SSSR, p. 3–22.

952 Khomentovsky, V.V., and Karlova, G.A., 1989, Vendian-Cambrian strata of the Dzhanda River and
953 their analogies in the key sections of eastern Siberia, *in* Khomentovsky, V.V. and Sovetov, Y.K.
954 eds., Late Precambrian and Early Palaeozoic of Siberia. Actual Problems of the Stratigraphy:
955 Novosibirsk, Insitut Geologii i Geofiziki, Sibirskoe Otdelenie, Akademiya Nauk SSSR, p. 23–61.

956 Khomentovsky, V.V., and Karlova, G.A., 1991, New data on the correlation of Vendian-Cambrian
957 strata in the eastern and trasitional facies regions of southern Yakutia., *in* Khomentovsky, V.V.
958 ed., Late Precambrian and Early Palaeozoic of Siberia. Siberian Platform and its Borderlands:
959 Novosibirsk, Ob'edinennyy Insitut Geologii, Geofiziki i Mineralogii, Sibirskoe Otdelenie,
960 Akademiya Nauk SSSR, p. 3–44.

961 Khomentovsky, V.V., and Karlova, G.A., 1993, Biostratigraphy of the Vendian-Cambrian beds and the
962 lower Cambrian boundary in Siberia: Geological Magazine, v. 130, p. 29–45.

963 Khomentovsky, V.V., and Karlova, G.A., 2002, The boundary between Nemakit-Daldynian and
964 Tommotian stages (Vendian-Cambrian Systems) of Siberia: Stratigraphy and Geological
965 Correlation, v. 10, p. 217–238.

966 Khomentovsky, V.V., and Karlova, G.A., 2005, The Tommotian Stage Base as the Cambrian Lower
967 Boundary in Siberia: Stratigraphy and Geological Correlation, v. 13, p. 21–34.

968 Khomentovsky, V.V., Val'kov, A.K., Karlova, G.A., and Nuzhnov, S.V., 1983, Key section of transitional
969 Precambrian-Cambrian strata in the lower Gonam River, *in* Khomentovsky, V.V. ed., Late
970 Precambrian and Early Palaeozoic of Siberia. Vendian Strata: Novosibirsk, Insitut Geologii i
971 Geofiziki, Sibirskoe Otdelenie, Akademiya Nauk SSSR, p. 24–36.

Khomentovsky, V.V., Val'kov, A.K., and Karlova, G.A., 1990, New data on the biostratigraphy of transitional Vendian-Cambrian strata in the middle Adan River basin, *in* Khomentovsky, V.V. and Gibsher, A.S. eds., Late Precambrian and Early Palaeozoic of Siberia. Problems of the Regional Stratigraphy: Novosibirsk, Insitut Geologii i Geofiziki, Sibirskoe Otdelenie, Akademiya Nauk SSSR, p. 3–57.

Khomentovsky, V. V., Postnikov, A.A., Karlova, G.A., Kochnev, B.B., Yakshin, M.S., and Ponomarchuk, V.A., 2004, The Vendian of the Baikal-Patom Upland, Siberia: Geologiya i Geofizika, v. 45, p. 465–484.

Kiselev, A.I., Kochnev, B.B., Yarmolyuk, V.V., Rogov, V.I., and Egorov, K.N., 2018, The early Paleozoic basite magmatism in the northeastern Siberian Craton: Geodynamics and Tectonophysics, v. 7, p. 233–250.

Knoll, A.H., Grotzinger, J.P., Kaufman, A.J., and Kolosov, P.N., 1995a, Integrated approaches to terminal Proterozoic stratigraphy: An example from the Olenek Uplift, northeastern Siberia: Precambrian Research, v. 73, p. 251–270.

Knoll, A.H., Kaufman, A.J., Semikhatov, M.A., Grotzinger, J.P., and Adams, W., 1995b, Sizing up the sub-Tommotian unconformity in Siberia: Geology, v. 23, p. 1139–1143.

Kochnev, B.B., Pokrovsky, B.G., Kuznetsov, A.B., and Marusin, V.V., 2018, C and Sr isotope chemostratigraphy of Vendian-Lower Cambrian carbonate sequences in the central Siberian Platform: Russian Geology and Geophysics, v. 59, p. 585–605.

Korshunov, V.I., Repina, L.N., and Sysoev, V.A., 1969, To the structure of the Pestrotsvet Formation on the East of the Aldan Anteclise: Geologiya i Geofizika, v. 1969(10), p. 18–21.

Kouchinsky, A., Bengtson, S., Pavlov, V., Runnegar, B., Val'kov, A., and Young, E., 2005, Pre-Tommotian age of the lower Pestrotsvet Formation in the Selinde section on the Siberian platform: carbon isotopic evidence: Geological Magazine, v. 142, p. 319–325.

996 Kouchinsky, A., Bengtson, S., Pavlov, V., Runnegar, B., Torssander, P., Young, E., and Ziegler, K., 2007,
997 Carbon isotope stratigraphy of the Precambrian-Cambrian Sukharikha River section,
998 northwestern Siberian platform: Geological Magazine, v. 114, p. 1–10.

999 Kouchinsky, A., Bengtson, S., Landing, E., Steiner, M., Vendrasco, M., and Ziegler, K., 2017,
1000 Terreneuvian stratigraphy and faunas from the Anabar Uplift, Siberia.: Acta Palaeontologica
1001 Polonica, v. 62, p. 311–440.

1002 Landing, E., Schmitz, M.D., Geyer, G., Trayler, R.B., and Bowring, S.A., 2020, Precise early Cambrian
1003 U-Pb zircon dates bracket the oldest trilobites and archaeocyaths in Moroccan West
1004 Gondwana: Geological Magazine, v. 158, p. 219–238.

1005 Linnemann, U. et al., 2019, New high-resolution age data from the Ediacran-Cambrian boundary
1006 indicate rapid, ecologically driven onset of the Cambrian explosion: Terra Nova, v. 31, p. 49–58.

1007 Macdonald, F.A., Strauss, J. V., Sperling, E.A., Halverson, G.P., Narbonne, G.M., Johnston, D.T.,
1008 Kunmann, M., Schrag, D.P., and Higgins, J.A., 2013, The stratigraphic relationship between the
1009 Shuram carbon isotope excursion, the oxygenation of Neoproterozoic oceans, and the first
1010 appearance of the Ediacara biota and bilaterian trace fossils in northwestern Canada: Chemical
1011 Geology, v. 362, p. 250–272.

1012 Magaritz, M., 1989, ^{13}C minima follow extinction events: A clue to faunal radiation: Geology, v. 17, p.
1013 337–340.

1014 Magaritz, M., Holser, W.T., and Kirschvink, J.L., 1986, Carbon-isotope events across the
1015 Precambrian/Cambrian boundary on the Siberian Platform: Nature, v. 320, p. 258–259.

1016 Malitch, N.S. et al., compilers, 1999, Geological map of Siberian Platform and adjoining areas: A.P.
1017 Karpinsky All-Russian Geological Research Institute, Ministry of Natural Resources of Russian
1018 Federation, scale 1:1,500,000, 9 sheets.

1019 Maloof, A.C., Schrag, D.P., Crowley, J.L., and Bowring, S.A., 2005, An expanded record of Early

1020 Cambrian carbon cycling from the Anti-Atlas Margin, Morocco: Canadian Journal of Earth
1021 Sciences, v. 42, p. 2195–2216.

1022 Maloof, A.C., Porter, S.M., Moore, J.L., Dudás, F.Ö., Bowring, S.A., Higgins, J.A., Fike, D.A., and Eddy,
1023 M.P., 2010a, The earliest Cambrian record of animals and ocean geochemical change:
1024 Geological Society of America Bulletin, v. 122, p. 1731–1774.

1025 Maloof, A.C., Ramezani, J., Bowring, S.A., Fike, D.A., Porter, S.M., and Mazouad, M., 2010b,
1026 Constraints on early Cambrian carbon cycling from the duration of the Nemakit-Daldynian–
1027 Tommotian boundary $\delta^{13}C$ shift, Morocco: Geology, v. 38, p. 623–626.

1028 Marusin, V.V., Kochnev, B.B., Karlova, G.A., and Nagovitsin, K.E., 2019, Resolving Terreneuvian
1029 stratigraphy in subtidal–intertidal carbonates: palaeontological and chemostratigraphical
1030 evidence from the Turukhansk Uplift, Siberian Platform: Lethaia, v. 52, p. 464–485.

1031 Marusin, V.V. et al., 2021, Detrital zircon age and biostratigraphic and chemostratigraphic
1032 constraints on the Ediacaran-Cambrian transitional interval in the Irkutsk Cis-Sayans Uplift,
1033 southwestern Siberian Platform: Geological Magazine, v. 158, p. 1156–1172.

1034 Matthews, S.C., and Cowie, J.W., 1979, Early Cambrian transgression: Journal of the Geological
1035 Society of London, v. 136, p. 133–135.

1036 McKie, T., 1993, Relative sea-level changes and the development of a Cambrian transgression:
1037 Geological Magazine, v. 130, p. 245–256.

1038 Mel'nikov, N. V. et al., 2005, Stratigraphy of the Oil-Gas-Bearing Basins of Siberia. Riphean and
1039 Vendian of the Siberian Platform and Its Folded Border: Novosibirsk, Academic Publishing
1040 House <Geo>, 428 p.

1041 Melim, L.A., Westphal, H., Swart, P.K., Eberli, G.P., and Munnecke, A., 2002, Questioning carbonate
1042 diagenetic paradigms: Evidence from the Neogene of the Bahamas: Marine Geology, v. 185, p.
1043 27–53.

1044 Merdith, A.S. et al., 2021, Extending full-plate tectonic models into deep time: Linking the
1045 Neoproterozoic and Phanerozoic: Earth-Science Reviews, v. 214, p. 103477.

1046 Narbonne, G.M., Kaufman, A.J., and Knoll, A.H., 1994, Integrated chemostratigraphy and
1047 biostratigraphy of the Windermere Supergroup, northwestern Canada: Implications for
1048 Neoproterozoic correlations and the early evolution of animals: Geological Society of America
1049 Bulletin, v. 106, p. 1281–1292.

1050 Nelson, L.L., Ahm, A.-S.C., Macdonald, F.A., Higgins, J.A., and Smith, E.F., 2021, Fingerprinting local
1051 controls on the Neoproterozoic carbon cycle with the isotopic record of Cryogenian carbonates
1052 in the Panamint Range, California: Earth and Planetary Science Letters, v. 566, p. 116956.

1053 Nelson, L.L., Ramezani, J., Almond, J.E., Darroch, S.A.F., Taylor, W.L., Brenner, D.C., Furey, R.P.,
1054 Turner, M., and Smith, E.F., 2022, Pushing the boundary: A calibrated Ediacaran-Cambrian
1055 stratigraphic record from the Nama Group in northwestern Republic of South Africa: Earth and
1056 Planetary Science Letters, v. 580, p. 117396.

1057 Parry, L.A. et al., 2017, Ichnological evidence for meiofaunal bilaterians from the terminal Ediacaran
1058 and earliest Cambrian of Brazil: Nature Ecology and Evolution, v. 1, p. 1455–1464.

1059 Pelechaty, S.M., 1998, Integrated chronostratigraphy of the Vendian System of Siberia: implications
1060 for a global stratigraphy: Journal of the Geological Society, London, v. 155, p. 957–973.

1061 Pelechaty, S.M., Grotzinger, J.P., Kashirtsev, V.A., and Zhernovsky, V.P., 1996a, Chemostratigraphic
1062 and sequence stratigraphic constraints on Vendian-Cambrian basin dynamics, Northeast
1063 Siberian Craton: The Journal of Geology, v. 104, p. 543–563.

1064 Pelechaty, S.M., Kaufman, A.J., and Grotzinger, J.P., 1996b, Evaluation of $\delta^{13}C$ chemostratigraphy for
1065 intrabasinal correlation: Vendian strata of northeast Siberia: Geological Society of America
1066 Bulletin, v. 108, p. 992–1003.

1067 Pokrovsky, B.G., Melezhik, V.A. and Bujakaite, M.I., 2006, Carbon, Oxygen, Strontium, and Sulfur

1068 Isotopic Compositions in Late Precambrian Rocks of the Patom Complex, Central Siberia:
1069 Communication 1. Results, Isotope Stratigraphy, and Dating Problems: Lithology and Mineral
1070 Resources, v. 41, p. 450–474.

1071 Pokrovsky, B.G., Bujakaite, M.I. and Kokin, O.V., 2012, Geochemistry of C, O, and Sr isotopes and
1072 chemostratigraphy of Neoproterozoic rocks in the northern Yenisei Ridge: Lithology and
1073 Mineral Resources, v. 47, p. 177–199.

1074 Pratt, B.R., Rule, R.G., 2021, A Mesoproterozoic carbonate platform (lower Belt Supergroup of
1075 western North America): Sediments, facies, tides, tsunamis and earthquakes in a tectonically
1076 active intracratonic basin, Earth-Science Reviews, v. 217, p. 103626.

1077 Pyatiletov, V.G., 1988, Late Precambrian microfossils of the Uchur-Maya Region, *in* Khomentovsky,
1078 V.V. and Shenfil', V.Y. eds., Late Precambrian and Early Palaeozoic of Siberia, Riphean and
1079 Vendian: Novosibirsk, Insitut Geologii i Geofiziki, Sibirskoe Otdelenie, Akademiya Nauk SSSR, p.
1080 47–104.

1081 Repina, L.N., Borodaevskaya, Z.V., and Ermak, V.V., 1988, Key section of the r. Selinde (south-eastern
1082 margin of the Aldan Shield), *in* Zhuravleva, I.T., and Repina, L.N., eds., Cambrian of Siberia and
1083 Middle Asia: Institut Geologii i Geofiziki, Sibirskoe Otdelenie, Akademiya Nauk SSSR, Trudy, v.
1084 720, p. 3–31 [in Russian].

1085 Rogov, V.I., Karlova, G.A., Marusin, V.V., Kochnev, B.B., Nagovitsin, K.E., and Grazhdankin, D.V., 2015,
1086 Duration of the first biozone in the Siberian hypostratotype of the Vendian: Russian Geology
1087 and Geophysics, v. 56, p. 573–583.

1088 Rozanov, A.Y., 1967, The Cambrian Lower Boundary Problem: Geological Magazine, v. 104, p. 415–
1089 434.

1090 Savitskiy, V.E., 1962, New data on the stratigraphy of the Aldanian Stage in the Anabar Anteclise and
1091 its boundary with the Precambrian., *in* Urvantsev, N.N. ed., Collection of Papers of the Institute

of Arctic Geology 27: Leningrad, Izdatel'stvo Nauchno-Issledovatel'skogo Instituta Geologii Arktiki, p. 14–21.

Saylor, B.Z., Kaufman, A.J., Grotzinger, J.P., and Urban, F., 1998, A composite reference section for terminal Proterozoic strata of southern Namibia: Journal of Sedimentary Research, v. 68, p. 1223–1235.

Semikhatov, M.A., Komar, V.A., and Serebryakov, S.N., 1970, Yudomian Complex of the Stratotypical Area: Geologicheskiy Institut, Academiya Nauk SSSR, Trudy, v. 210, p. 1–207.

Semikhatov, M.A., Obchinnikova, G.V., Gorokhov, I.M., Kuznetsov, A.B., Kaurova, O.K., and Petrov, P.Y., 2003, Pb-Pb Isochron Age and Sr-Isotopic Signature of the Upper Yudoma Carbonate Sediments (Vendian of the Yudoma-Maya Trough, Eastern Siberia): Doklady Earth Sciences, v. 393, p. 1093–1097.

Smith, E.F., Macdonald, F.A., Petach, T.A., Bold, U., and Schrag, D.P., 2016a, Integrated stratigraphic, geochemical, and paleontological late Ediacaran to early Cambrian records from southwestern Mongolia: Geological Society of America Bulletin, v. 128, p. 442–468.

Smith, E.F., Nelson, L.L., Strange, M.A., Eyster, A.E., Rowland, S.M., Schrag, D.P., and Macdonald, F.A., 2016b, The end of the Ediacaran: Two new exceptionally preserved body fossil assemblages from Mount Dunfee, Nevada, USA: Geology, v. 44, p. 911–914.

Sovetov, J.K., 2002, Vendian foreland basin of the Siberian cratonic margin: Paleopangean accretionary phases: Russian Journal of Earth Sciences, v. 4, p. 363–387.

Sukhov, S.S., Pegel', T.V., and Shabanov, Yu.Ya., 2021, Regional Stratigraphic Chart of Cambrian Strata of the Siberian Platform, Explanatory Note, Resolutions of All-Russian Stratigraphic Meeting on the Development of Stratigraphic Charts of the Upper Precambrian and Paleozoic of Siberia (Novosibirsk, 2012), Cambrian of the Siberian Platform: Novosibirsk, Sibirskiy Nauchno-Issledovate'skiy Institut Geologii, Geofiziki i Mineral'nogo Syr'ya, 60 p.

1116 Topper, T., Betts, M.J., Dorjnamjaa, D., Li, G., Li, L., Altanshagai, G., Enkhbaatar, B., and Skovsted,
1117 C.B., 2022, Locating the BACE of the Cambrian: Bayan Gol in southwestern Mongolia and global
1118 correlation of the Ediacaran-Cambrian boundary: Earth-Science Reviews, v. 229, p. 104017.

1119 Val'kov, A.K., 1983, Distribution of the oldest skeletal organisms and the correlation of the Cambrian
1120 lower boundary in the south-eastern part of the Siberian Platform, *in* Khomentovsky, V.V. ed.,
1121 Late Precambrian and Early Palaeozoic of Siberia, Vendian Strata: Novosibirsk, Insitut Geologii i
1122 Geofiziki, Sibirskoe Otdelenie, Akademiya Nauk SSSR, p. 37–48.

1123 Val'kov, A.K., and Karlova, G.A., 1984, Fauna from transitional Vendian-Cambrian strata in the lower
1124 Gonam River, *in* Khomentovsky, V.V. ed., Stratigraphy of the Late Precambrian and Early
1125 Palaeozoic. Middle Siberia: Novosibirsk, Insitut Geologii i Geofiziki, Sibirskoe Otdelenie,
1126 Akademiya Nauk SSSR, p. 12–41.

1127 Veizer, J., and Hoefs, J., 1976, The nature of $^{18}O/^{16}O$ and $^{13}C/^{12}C$ secular trends in sedimentary
1128 carbonate rocks: Geochimica et Cosmochimica Acta, v. 40, p. 1387–1395.

1129 Veizer, J., Holser, W.T., and Wilgus, C.K., 1980, Correlation of $^{13}C/^{12}C$ and $^{34}S/^{32}S$ secular variations:
1130 Geochimica et Cosmochimica Acta, v. 44, p. 579–587.

1131 Vologdin, A.G., and Maslov, A.B., 1960, On a new group of fossil organisms from the lower Yudoma
1132 Formation of the Siberian Platform: Doklady Akademii Nauk SSSR, v. 134, p. 691–693.

1133 Wood, R., Ivantsov, A.Y., and Zhuravlev, A.Y., 2017a, First macrobiota biomineralization was
1134 environmentally triggered: Proceedings of the Royal Society B: Biological Sciences, v. 284, p.
1135 20170059.

1136 Wood, R.A., Zhuravlev, A.Y., Sukhov, S.S., Zhu, M., and Zhao, F., 2017b, Demise of Ediacaran
1137 dolomitic seas marks widespread biomineralization on the Siberian Platform: Geology, v. 45, p.
1138 27–30.

1139 Wood, R.A., Liu, A.G., Bowyer, F.T., Wilby, P.R., Dunn, F.S., Kenchington, C.G., Hoyal Cuthill, J.F.,

Mitchell, E.G., and Penny, A.M., 2019, Integrated records of environmental change and evolution challenge the Cambrian Explosion: Nature Ecology and Evolution, v. 3, p. 528–538.

Yakshin, M.S., and Pereverzev, L.R., 1990, The Yudoma Group in the upper Maya River basin, *in* Khomentovsky, V.V., and Gibsher, A.S., eds., Late Precambrian and Early Palaeozoic of Siberia. Problems of the Regional Stratigraphy: Novosibirsk, Institut Geologii i Geofiziki, Sibirskoe Otdelenie, Akademiya Nauk SSSR, p. 58–63 [in Russian].

Yang, C., Rooney, A.D., Condon, D.J., Li, X.-H., Grazhdankin, D. V., Bowyer, F.T., Hu, C., Macdonald, F., and Zhu, M., 2021, The tempo of Ediacaran evolution: Science Advances, v. 7, p. eabi9643.

Zhu, M.-Y., Babcock, L.E., and Peng, S.-C., 2006, Advances in Cambrian stratigraphy and paleontology: Integrating correlation techniques, paleobiology, taphonomy and paleoenvironmental reconstruction: Palaeoworld, v. 15, p. 217–222.

Zhu, M., Zhang, J., and Yang, A., 2007, Integrated Ediacaran (Sinian) chronostratigraphy of South China: Palaeogeography, Palaeoclimatology, Palaeoecology, v. 254, p. 7–61.

Zhu, M., Zhuravlev, A.Y., Wood, R.A., Zhao, F., and Sukhov, S.S., 2017, A deep root for the Cambrian explosion: Implications of new bio- and chemostratigraphy from the Siberian Platform: Geology, v. 45, p. 459–462.

Zhu, M., Yang, A., Yuan, J., Li, G., Zhang, J., Zhao, F., Ahn, S.-Y., and Miao, L., 2019, Cambrian integrative stratigraphy and timescale of China: Science China Earth Sciences, v. 62, p. 25–60.

Zhuravlev, A.Y., 1998, Outlines of the Siberian Platform sequence stratigraphy in the lower and lower middle Cambrian (Lena-Aldan area): Revista Española de Paleontología, no. extr., p. 103–112.

Zhuravlev, A.Yu., and Naimark, E.B., 2005, Alpha, beta, or gamma: Numerical view on the Early Cambrian world. Palaeogeography, Palaeoclimatology, Palaeoecology, v. 220, p. 207–225.

Zhuravlev, A.Y., Gámez Vintaned, J.A., and Ivantsov, A.Y., 2009, First finds of problematic Ediacaran

fossil *Gaojiashania* in Siberia and its origin: Geological Magazine, v. 146, p. 775–780.

FIGURE CAPTIONS

Figure 1. Map of the Siberian Platform with major pre-Cambrian to lower Cambrian study regions (after Astashkin et al., 1991; Sovetov, 2002; Khomentovsky, 2008). Details and references for each section are provided in the high-resolution stratigraphic correlation charts presented in Figs. S1–S7. Major pre-Cambrian to Cambrian study areas: (I) Yenisei Range, (II) Irkutsk Amphitheatre and Baikal and Patom highlands, (III) Syugdzhera Saddle (Nepa-Botuoba Uplift to southern slope of Anabar Shield), (IV) Igarka-Norilsk Uplift, (V) Anabar Shield, (VI) Olenek Uplift, (VII) Khara-Ulakh Mountains, (VIII) Lena River, (IX) Uchur-Maya Plate, (X) Yudoma-Maya Belt, (XI) Okhotsk Microcontinent. Markers point to the precise location of individual sections.

Figure 2. Summarized stratigraphic subdivision and nomenclature of the Siberian Platform by study region, from the middle Ediacaran (ca. 575 Ma) to late Stage 3 of the Cambrian. The geographic positions of individual study regions are provided in Fig. 1. Bold horizontal lines mark major (often erosional or karstified) sequence boundaries. Formations correlated using litho-, bio- and chemostratigraphy after numerous publications referenced in the text and provided in Figs. S1–S7. Question marks represent uncertainty in the duration of the hiatus between the Tolba/Ust'-Yudoma and Pestrotvet formations.

Figure 3. Regional map and stratigraphic information for sections along the Yudoma River of the southeastern Siberian Platform. (A) Overview map of the Siberian Platform (see Figs 1 and S1–S7 for details of major study regions I-X), (B) Detailed map of the Yudoma River area (drafted using the 1:1,500,000 Geological map of the Siberian Platform and adjoining areas by

1186 Malitch et al., 1999), (C) Yudoma-Maya confluence section, lower part, (D) Nuuchchalakh
1187 valley section, and (E) Kyra-Ytyga River mouth section. Carbon isotope data, biozones, and
1188 stratigraphy for KY have previously been published in Zhu et al. (2017) but are included here
1189 for completion of the shelf transect. Horizontal dotted lines with Roman numerals show precise
1190 levels of associated SSF assemblages (see legend for constituent fossils).

1191 Figure 4. Outcrop photographs (A–C) Yudoma-Maya confluence (YM), and (D–J)
1192 Nuuchchalakh valley (NV). (A) Panorama of the Aim and lower Ust'-Yudoma formations at
1193 YM, (B) sampled section at YM, and (C) stylolitized horizon below the karst surface near the
1194 top of the '*Suvorovella* shell bed' containing reworked fragments of *Suvorovella*, scale bar =
1195 10 cm. (D) Panorama of the NV section. (E) The Aim and lowermost Ust'-Yudoma formations
1196 at NV. (F) Dolomite and siltstone of the basal Aim Formation overlay dark sediments of the
1197 Ust'-Kirbi Formation at NV. (G) Stromatolitic horizon near the top of the Aim Formation at
1198 NV. (H) Undulose contact between flaggy dolomite and siltstone of the upper Aim Formation,
1199 and massive dolomite of the lowermost Ust'-Yudoma Formation at NV. (I) Intraformational
1200 breccia near the base of the Ust'-Yudoma Formation at NV. (J) Silty dolostone and darker
1201 ribbon-like laminae in the lower Ust'-Yudoma Formation at NV. This ribbon-rock constitutes
1202 common brecciated clasts in the intraformational breccia. Yellow, white, and black arrows in
1203 (D–F, H) mark the levels of the basal Aim Formation, the sequence boundary in the middle
1204 Aim Formation, and the contact between the Aim and Ust'-Yudoma formations, respectively.

1205 Figure 5. Outcrop photographs of the Kyra-Ytyga River mouth (KY) section. (A,B) Panorama
1206 photographs to show outcrop of the Ust'-Kirbi, Aim, and Ust'-Yudoma formations at KY. (C)
1207 Thinly laminated organic-rich limestone of the upper Aim Formation. (D) Sharp contact
1208 between thin bedded limestone of the upper Aim Formation and massive dolostone of the Ust'-

1209 Yudoma Formation. Yellow and black arrows in (A,B,D) mark the levels of the basal Aim
1210 Formation, and the contact between the Aim and Ust'-Yudoma formations, respectively.

1211 Figure 6. SEM images and photographs of fossils from the Ust'-Yudoma Formation, Kyra-
1212 Ytyga River mouth (Zhu et al., 2017). Fossil assemblage horizons after Zhu et al. (2017). Level
1213 II: (A) Cloudinidae gen. et sp. indet., (B-C) *Cloudina* ex gr. *riemkeae*, (D-E) *Anabarites*
1214 *valkovi*, (F-G) *A. trisulcatus*. Scale bar: 200 μm (A-E, F), 100 μm (G). Collection: A. B.
1215 Fedorov. Level III: (A) anabaritid, (B) *Anabarites trisulcatus*, (C-D) *Cambrotubulus*
1216 *decurvatus*. Scale bar: 1 mm. Photography: MZ and FZ. Level IV: (A) *Protohertzina*
1217 *unguliformis*, (B) Cloudinidae gen. et sp. indet., (C) *Anabarites latus*, (D) *A. natellus*, (E) *A.*
1218 *tripartitus*, (F) *Cambrotubulus decurvatus*. Scale bar: 50 μm (A), 100 μm (B-E), 150 μm (F).
1219 Collections: (A, C-F) Yu. Ya. Shabanov, (B) A. B. Fedorov. Level V: (A) *Cambrotubulus*
1220 *decurvatus*, (B) *Protohertzina*? *anabarica*, (C) Chancelloriidae gen. et sp. indet., (D)
1221 *Fomitchella infundibuliformis*, (E) *F. acinaciformis*, (F) *Halkieria* sp., (G) *Sachites* sp., (H)
1222 *Hyolithellus tenuis*. Scale bar: 120 μm (A), 50 μm (B, G, H), 200 μm (C), 100 μm (D).
1223 Collections: (A, B, D-H) Yu. Ya. Shabanov, (C) V. V. Khomentovsky. Specimens of levels II,
1224 IV, and V were photographed by A. B. Fedorov.

1225 Figure 7. Cross-plots of carbon and oxygen isotopes separated by mineralogy for (A) compiled
1226 data of the Siberian Platform, (B) the Ust'-Yudoma Formation at NV, (C) the Ust'-Yudoma
1227 Formation at KY, (D) the Aim Formation at YM, (E) the Aim Formation at NV, and (F) the
1228 Aim Formation at KY. The shapes of individual data points in the NV section (B,E) are as
1229 described in Fig. 3D.

1230 Figure 8. High resolution lithostratigraphic, chemostratigraphic and biostratigraphic
1231 correlation chart for sections of the southeast Siberian Platform. Uncertainty in the nature of
1232 the boundary between the Aim and Ust'-Yudoma formations is shows as a red dashed line.

Inset map shows positions of exposed river bank sections on the Uchur-Maya Plate and Yudoma-Maya Belt. Detailed bed-by-bed descriptions of sections 1 to 9 are provided in the supplementary material. This figure is reproduced at higher resolution and with additional sections, in Fig. S7. Chemostratigraphy of Dvortsy section, Aldan River after Magaritz et al. (1986) and Brasier et al. (1993); chemostratigraphy of the Kyra-Ytyga River mouth after Zhu et al. (2017); fossil data, lithostratigraphic correlation, and member designation in the Ust'-Yudoma Formation after Khomentovsky (1985, 2008), Khomentovsky and Karlova (1986, 1989, 1991, 1993), Khomentovsky et al. (1983, 1990), Semikhatov et al. (1970), Val'kov (1983), Val'kov and Karlova (1984), and Yakshin and Pereverzev (1990).

Figure 9. Schematic representations of alternative depositional models for sections between Dvortsy and KY. Model E (A–C) assumes no depositional hiatus at the boundary between the Aim and Ust'-Yudoma formations, resulting in a pre-1n/BACE correlation for the Ust'-Yudoma Formation in sections of the Yudoma River. Model F (D–F) assumes a significant depositional hiatus at the Formation boundary and results in a post-1n/BACE correlation for the Ust'-Yudoma Formation in sections of the Yudoma River.

Figure 10. Summarized litho-, chemo-, and sequence stratigraphic correlation of selected late Ediacaran sections of the Siberian Platform. Figure shows a possible lithostratigraphic correlation between sections of the Olenek Uplift and the Yudoma River, assuming continuous depositional across the boundary between the Aim and Ust'-Yudoma formations (Model E). Litho-, bio- and chemostratigraphy of the Olenek Uplift and Khara-Ulakh Mountains after Pelechaty et al. (1996a), Knoll et al. (1995), Rogov et al. (2015) and Cui et al. (2016). Section correlation and sequence stratigraphy between the Olenek Uplift and Khara-Ulakh Mountains after Pelechaty et al. (1996a,b). Note that correlation between the Khatypsyt and Kharayutekh formations remains uncertain. Tentative $\delta^{13}C_{carb}$ peak correlation [A4–5p] follows best-fit

visual alignment to $\delta^{13}C_{carb}$ excursions of possible global significance, as discussed in the text. A4 = negative $\delta^{13}C_{carb}$ excursion in the A4 Member of the Ara Group, Oman, SPIE = Spitskop $\delta^{13}C_{carb}$ excursion, 0n = possible minor negative $\delta^{13}C_{carb}$ excursion between 1p and 1n/BACE. Detailed section information and alternative peak correlations for pre-1n/BACE strata are presented in Fig. S5.

Figure 11. Summarized litho-, chemo-, and sequence stratigraphic correlation of selected sections of the Siberian Platform that host the 1n/BACE relative to the Yudoma River sections. Model E assumes a pre-1n/BACE correlation for the Yudoma River sections, whilst Model F correlates the Ust'-Yudoma Formation along the Yudoma River to the Fortunian (see text for discussion). Key provided in Fig. 10. Lithostratigraphic and chemostratigraphic information: Irkut River: Marusin et al. (2020), Nokhtuysk: Pelechaty (1998), Sukharikha: Kouchinsky et al. (2007), Kotuykan: Knoll et al. (1995b); Kaufman et al. (1996), Dvortsy: Magaritz et al. (1986); Brasier et al. (1993), Ulakhan-Sulugur: Magaritz (1989); Brasier et al. (1993), Selinde: Korshunov et al. (1969); Repina et al. (1998); Khomentovsky and Karlova (2002); Kouchinsky et al. (2005), Kyra-Ytyga River mouth: Zhu et al. (2017). Detailed section information and additional correlations are presented in Figs. S1–S7.

Figure 12. Best-fit visual alignment of Siberian composite $\delta^{13}C_{carb}$ reference curves to radiometrically calibrated global $\delta^{13}C_{carb}$. Scaffold of radiometrically calibrated global data is updated from Bowyer et al. (2022) with new data from the Nama Group after Nelson et al. (2022). Siberian reference curves after (A) Model E, and (B) Model F. Acronyms A3–VIII correspond with $\delta^{13}C_{carb}$ excursions of possible global significance (Brasier et al., 1994b; Maloof et al., 2010a; Bowyer et al., 2022). SINSK corresponds to the partial extinction of archaeocyaths coincident with transgression and deposition of the Sinsk Formation along the Lena River, and equivalent platform-wide formations. Panels (C) to (E) show the migrating

pattern of facies zones and belts that result from models E and F in the interval prior to the 1n/BACE (C), throughout the Fortunian Stage (D), and through the Tommotian to Atdabanian stages (E). Drafted using paleofacies maps after Sukhov et al. (2021) and section correlations employed herein.

Figure 13. Age model output for global SSF biostratigraphy (updated from Bowyer et al. 2022). (A) 1. Ediacaran-Cambrian boundary ca. 538.8 Ma (ICC2022) after maximum age for the FAD of *T. pedum* based on lithostratigraphic correlation to section hosting radiometric age (Namibia, see discussions in Bowyer et al., 2022; Nelson et al., 2022; and herein); 2. 1n/BACE nadir after Model C of Bowyer et al. (2022); 3. Chemostratigraphically constrained maximum age for the FAD of *T. pedum* in the Esmeralda Member of the Deep Spring Formation, Mount Dunfee Section, Nevada, USA (Laurentia, Smith et al., 2016b). Best-fit visual alignment of $\delta^{13}C_{carb}$ data calibrates associated biostratigraphy after (B) Model E, and (C) Model F. All $\delta^{13}C_{carb}$ models include radiometrically calibrated and best-fit global data, colour coded by region and updated with new data from the Kalahari craton, South Africa (Nelson et al., 2022), the Zavkhan terrane, Mongolia (Topper et al., 2022), and the southeast Siberian Platform (herein). The ZHUCE in the Dahai Member of South China is assumed to correlate with 6p in this model. Dashed vertical lines indicate uncertain range extensions. Single fragment of ?*Barskovia* sp. in the lower Platonovka Formation at Sukhaya Tunguska section may represent the earliest occurrence of stem group mollusks (Marusin et al., 2019). Historical biostratigraphic information from the Zuun-Arts and Bayan Gol formations of the Zavkhan Terrane, Mongolia (as presented in Bowyer et al., 2022) is replaced herein by the chemostratigraphically-calibrated biostratigraphy of Topper et al. (2022). Fossil occurrences in the phosphatic Zhongyicun Member of South China are not considered. (D) Temporal range of cloudinids according to models E and F, including (i) cloudinids recorded in the middle Ust'-Yudoma Formation at KY, and (ii) chemostratigraphically well-constrained *Zuunia chimidtsereni* in the

Zuun-Arts and lower Bayan Gol formations (Topper et al., 2022). Full age model spreadsheet available upon request.

[1]Supplemental Material. *[Supplementary text, Table S1 and figures S1-S7]* Please visit https://doi.org/10.1130/XXXX to access the supplemental material, and contact editing@geosociety.org with any questions.

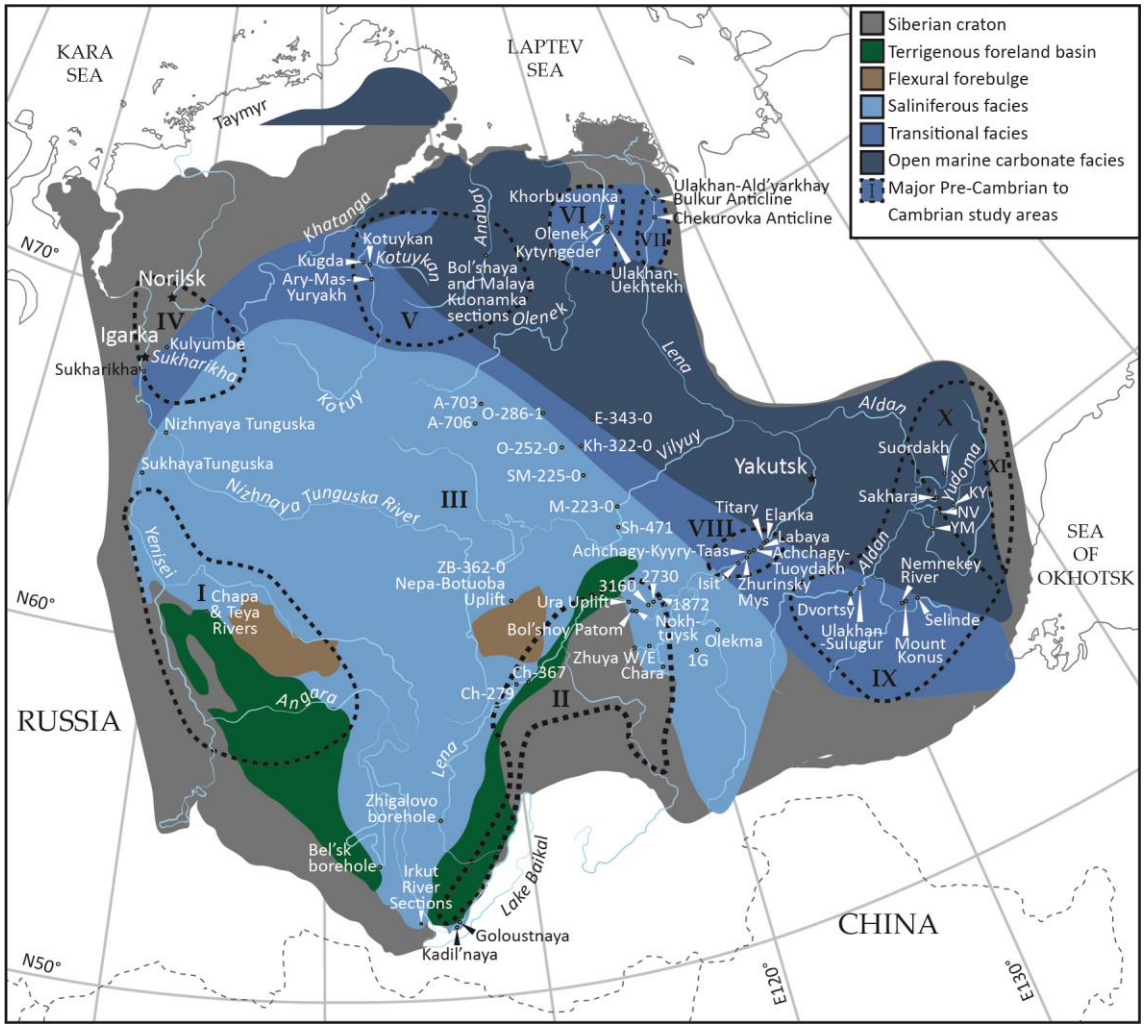
Siberian craton
Terrigenous foreland basin
Flexural forebulge
Saliniferous facies
Transitional facies
Open marine carbonate facies
Major Pre-Cambrian to Cambrian study areas
KARA SEA
LAPTEV SEA
SEA OF OKHOTSK
RUSSIA
CHINA
Taymyr
Khatanga
Anabar
Khorbusuonka
Ulakhan-Ald'yarkhay
Bulkur Anticline
Chekurovka Anticline
Kotuykan
Kotuykan
Olenek
Kytyngeder
Kugda
Ary-Mas-Yuryakh
Bol'shaya and Malaya Kuonamka sections
Olenek
Ulakhan-Uekhtekh
Norilsk
Igarka
Kulyumbe
Sukharikha
Sukharikha
Lena
Kotuy
A-703
A-706
O-286-1
E-343-0
Nizhnyaya Tunguska
O-252-0
Kh-322-0
Vilyuy
Aldan
Suordakh
Yudoma
SukhayaTunguska
SM-225-0
Yakutsk
Nizhnaya Tunguska River
M-223-0
Titary
Elanka
Sakhara
KY
NV
YM
Sh-471
Labaya
Achchagy-Kyyry-Taas
Achchagy-Tuoydakh
Yenisei
ZB-362-0
Nepa-Botuoba Uplift
3160
2730
Isit
Zhurinsky Mys
Aldan
Nemnekey River
Chapa & Teya Rivers
Ura Uplift
1872
Dvortsy
Selinde
Bol'shoy Patom
Nokh-tuysk
Olekma
Ulakhan-Sulugur
Mount Konus
Zhuya W/E Chara
1G
Ch-367
Ch-279
Angara
Lena
Zhigalovo borehole
Bel'sk borehole
Irkut River Sections
Lake Baikal
Goloustnaya
Kadil'naya
N70°
N60°
N50°
E120°
E130°

1312

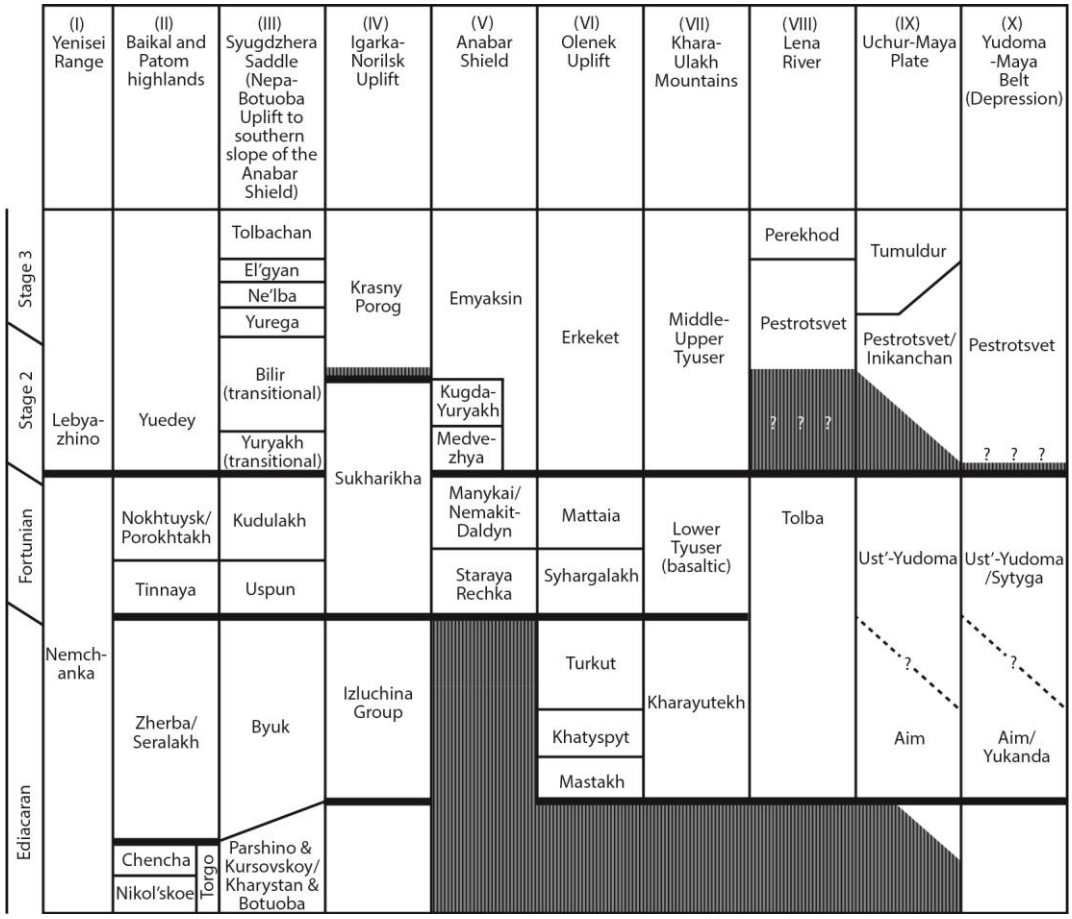
(I) Yenisei Range
(II) Baikal and Patom highlands
(III) Syugdzhera Saddle (Nepa-Botuoba Uplift to southern slope of the Anabar Shield)
(IV) Igarka-Norilsk Uplift
(V) Anabar Shield
(VI) Olenek Uplift
(VII) Khara-Ulakh Mountains
(VIII) Lena River
(IX) Uchur-Maya Plate
(X) Yudoma -Maya Belt (Depression)
Stage 3
Stage 2
Fortunian
Ediacaran
Tolbachan
El'gyan
Ne'lba
Yurega
Bilir (transitional)
Yuryakh (transitional)
Krasny Porog
Emyaksin
Erkeket
Middle-Upper Tyuser
Perekhod
Pestrotsvet
Tumuldur
Pestrotsvet/ Inikanchan
Pestrotsvet
Lebya-zhino
Yuedey
Kugda-Yuryakh
Medve-zhya
Sukharikha
Nokhtuysk/ Porokhtakh
Kudulakh
Tinnaya
Uspun
Manykai/ Nemakit-Daldyn
Staraya Rechka
Mattaia
Syhargalakh
Lower Tyuser (basaltic)
Tolba
Ust'-Yudoma
Ust'-Yudoma /Sytyga
Nemch-anka
Zherba/ Seralakh
Byuk
Izluchina Group
Turkut
Khatyspyt
Mastakh
Kharayutekh
Aim
Aim/ Yukanda
Chencha
Nikol'skoe
Torgo
Parshino & Kursovskoy/ Kharystan & Botuoba

1313

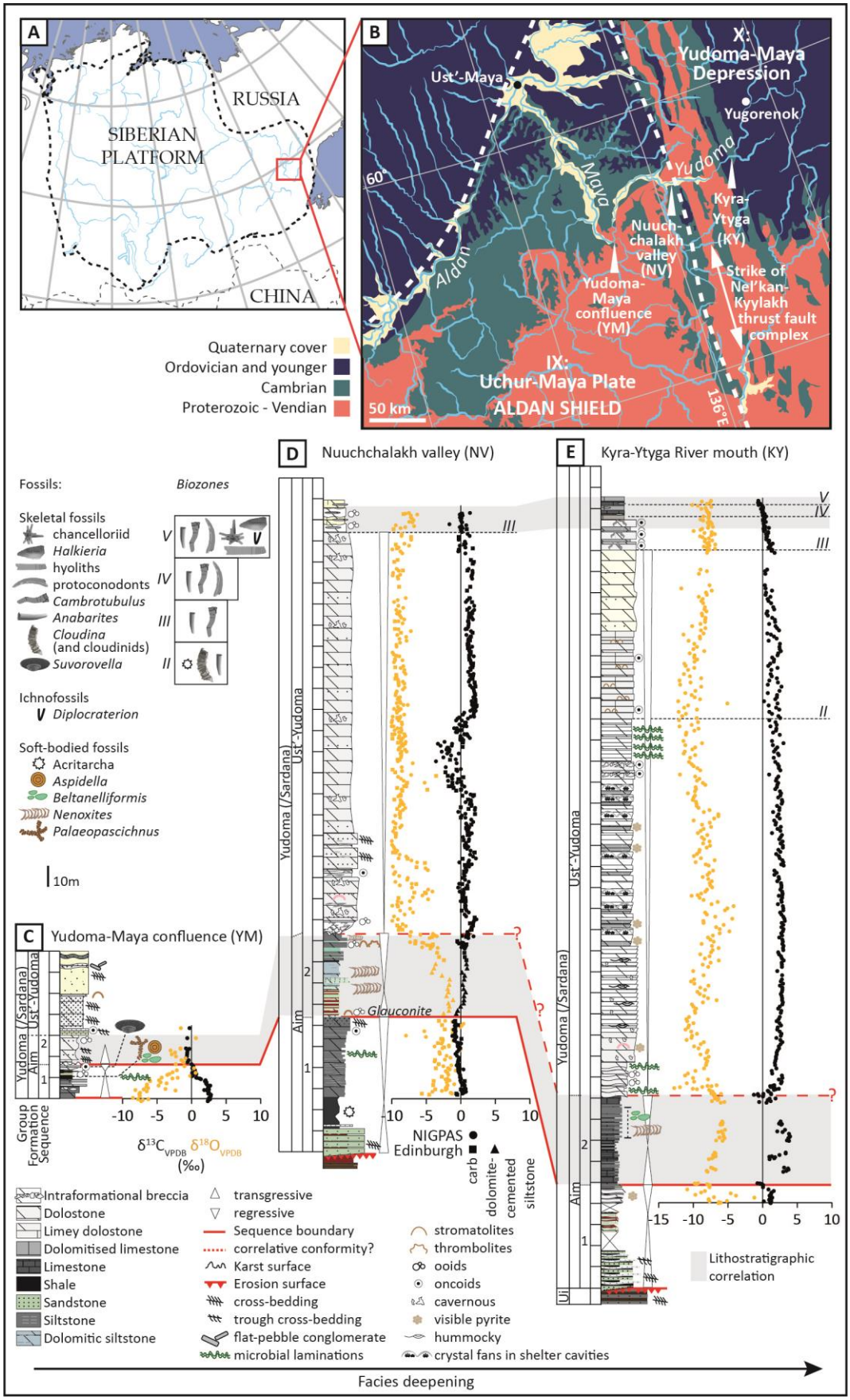
A
RUSSIA
SIBERIAN PLATFORM
CHINA
B
X: Yudoma-Maya Depression
Ust'-Maya
Yugorenok
Maya
Yudoma
60°
Kyra-Ytyga (KY)
Nuuch-chalakh valley (NV)
Aldan
Yudoma-Maya confluence (YM)
Strike of Nel'kan-Kyylakh thrust fault complex
IX: Uchur-Maya Plate
ALDAN SHIELD
50 km
136°E
Quaternary cover
Ordovician and younger
Cambrian
Proterozoic - Vendian
D Nuuchchalakh valley (NV)
E Kyra-Ytyga River mouth (KY)
Fossils:
Biozones
Skeletal fossils
chancelloriid
Halkieria
hyoliths
protoconodonts
Cambrotubulus
Anabarites
Cloudina (and cloudinids)
Suvorovella
Ichnofossils
Diplocraterion
Soft-bodied fossils
Acritarcha
Aspidella
Beltanelliformis
Nenoxites
Palaeopascichnus
10m
C Yudoma-Maya confluence (YM)
Yudoma (/Sardana)
Ust'-Yudoma
Aim
Group
Formation
Sequence
δ13CVPDB δ18OVPDB (‰)
Glauconite
NIGPAS
Edinburgh
carb
dolomite-cemented siltstone
Lithostratigraphic correlation
Intraformational breccia
Dolostone
Limey dolostone
Dolomitised limestone
Limestone
Shale
Sandstone
Siltstone
Dolomitic siltstone
transgressive
regressive
Sequence boundary
correlative conformity?
Karst surface
Erosion surface
cross-bedding
trough cross-bedding
flat-pebble conglomerate
microbial laminations
stromatolites
thrombolites
ooids
oncoids
cavernous
visible pyrite
hummocky
crystal fans in shelter cavities
Facies deepening

1314

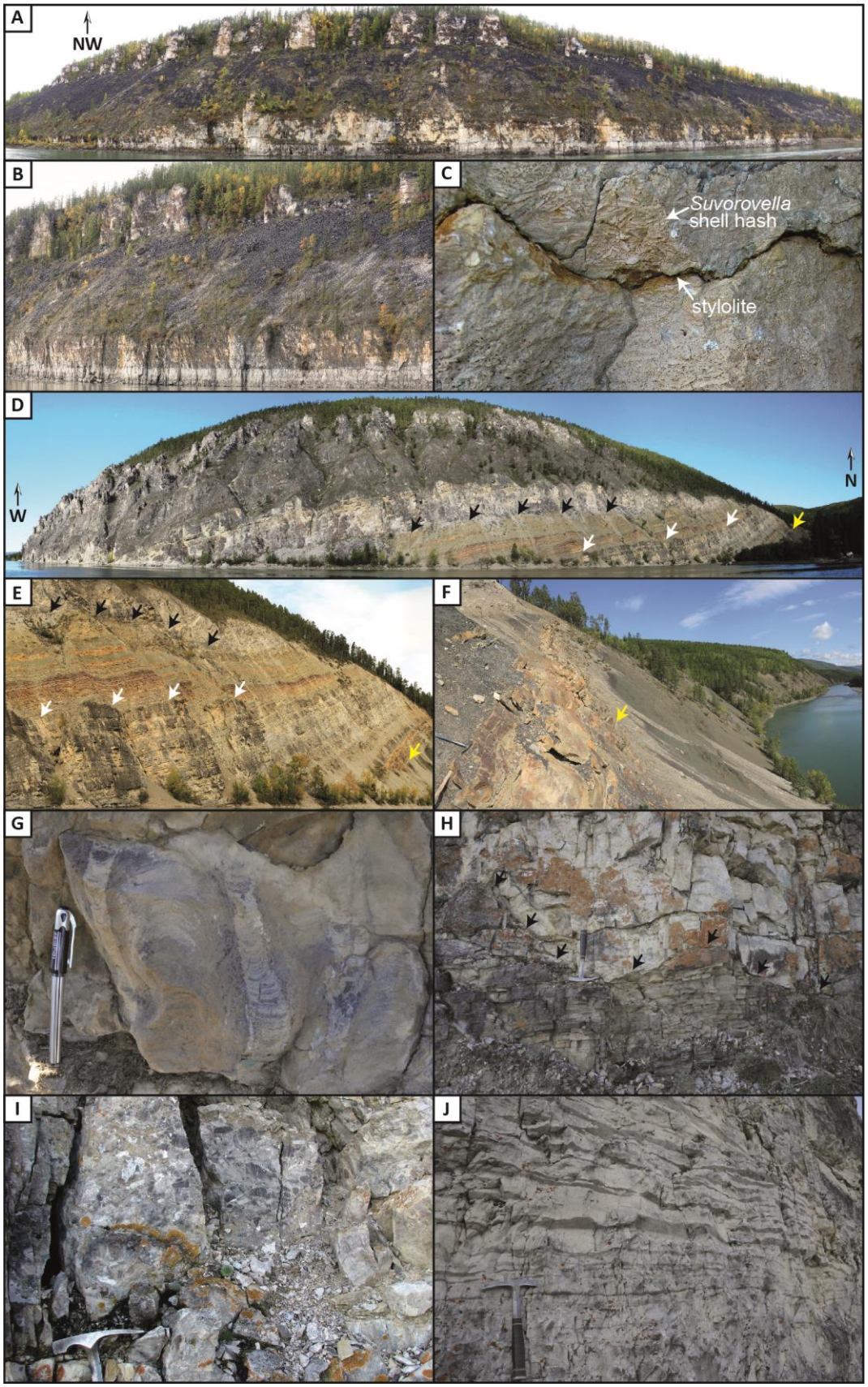

1315

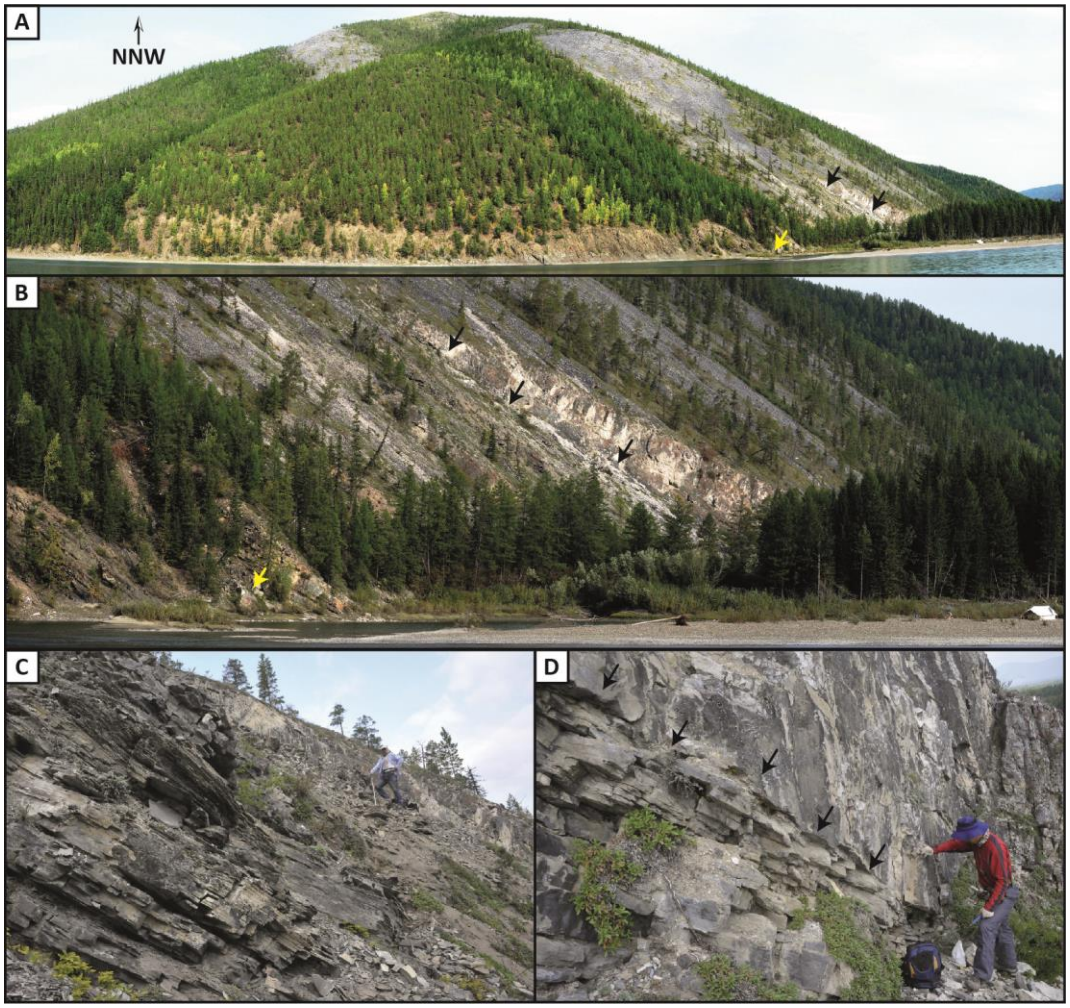

1316

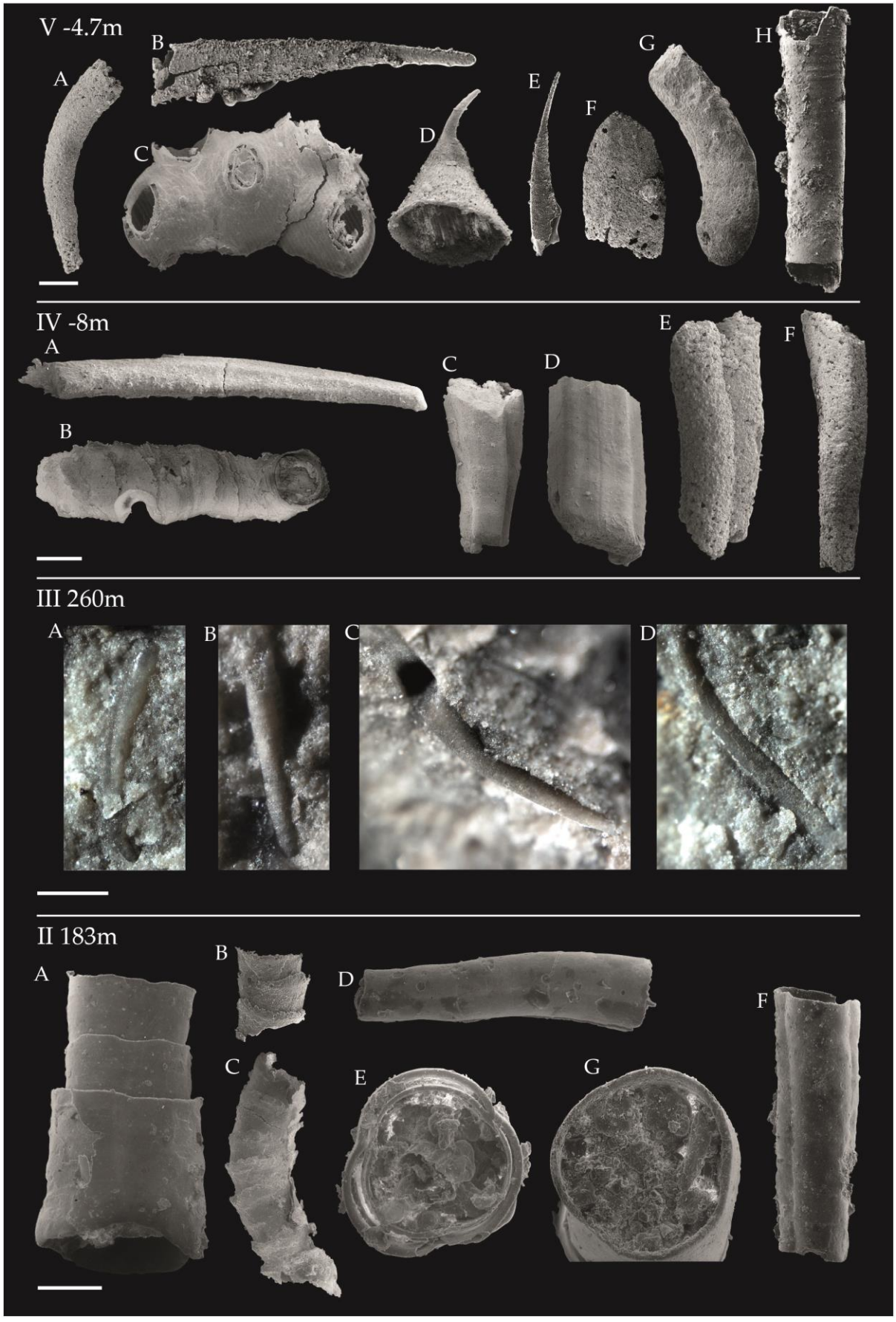

1317

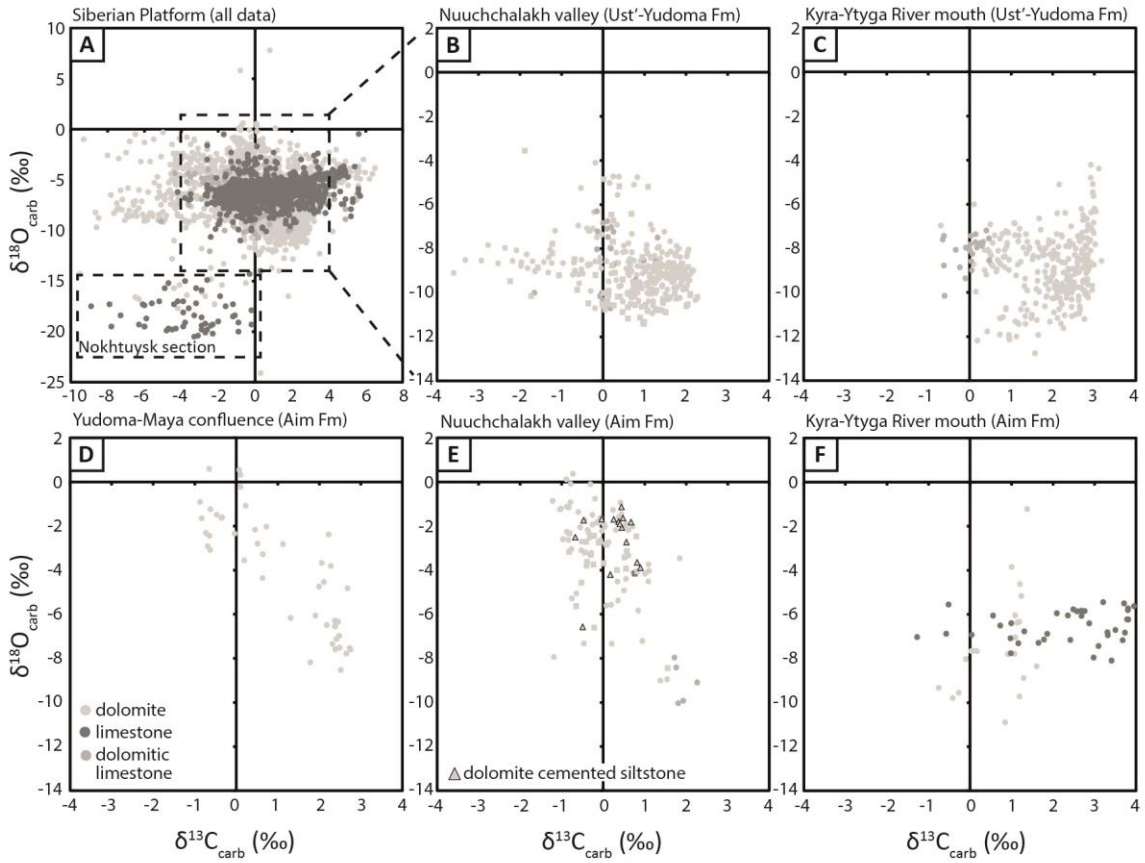
Siberian Platform (all data)
A
Nokhtuysk section
Nuuchchalakh valley (Ust'-Yudoma Fm)
B
Kyra-Ytyga River mouth (Ust'-Yudoma Fm)
C
Yudoma-Maya confluence (Aim Fm)
D
Nuuchchalakh valley (Aim Fm)
E
Kyra-Ytyga River mouth (Aim Fm)
F
δ18Ocarb (‰)
δ13Ccarb (‰)
dolomite
limestone
dolomitic limestone
dolomite cemented siltstone

1318

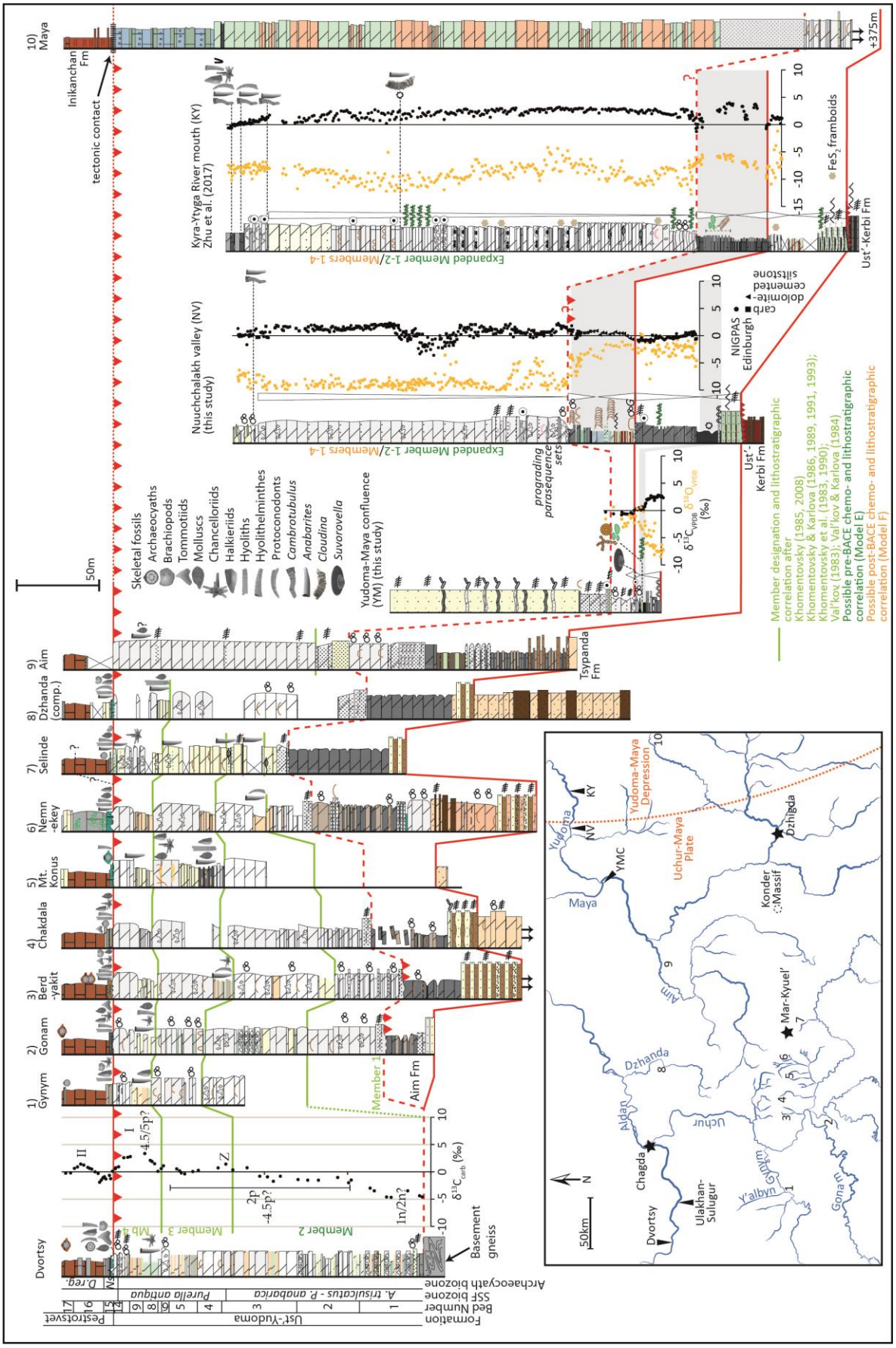
10) Maya
Inikanchan Fm
tectonic contact
+375m
Kyra-Ytyga River mouth (KY)
Zhu et al. (2017)
Expanded Member 1-2/Members 1-4
Ust'-Kerbi Fm
FeS2 framboids
Nuuchchalakh valley (NV)
(this study)
NIGPAS
Edinburgh
carb ● ■ dolomite-cemented siltstone
prograding parasequence sets
Yudoma-Maya confluence (YM) (this study)
Skeletal fossils
Archaeocyaths
Brachiopods
Tommotiids
Molluscs
Chancelloriids
Halkieriids
Hyoliths
Hyolithelminthes
Protoconodonts
Cambrotubulus
Anabarites
Cloudina
Suvorovella
50m
9) Aim
8) Dzhanda (comp.)
Tsypanda Fm
7) Selinde
6) Nemn -ekey
5) Mt. Konus
4) Chakdala
3) Berd -yakit
2) Gonam
1) Gynym
Member 1
Aim Fm
Member 2
Member 3
Mb 4
Basement gneiss
Dvortsy
Member designation and lithostratigraphic correlation after
Khomentovsky (1985, 2008)
Khomentovsky & Karlova (1986, 1989, 1991, 1993);
Khomentovsky et al. (1983, 1990);
Val'kov (1983); Val'kov & Karlova (1984)
Possible pre-BACE chemo- and lithostratigraphic correlation (Model E)
Possible post-BACE chemo- and lithostratigraphic correlation (Model F)
Yudoma
Maya
Aim
Aldan
Uchur
Gonam
Yudoma-Maya Depression
Uchur-Maya Plate
Konder Massif
Dzhida
Mar-Kyuel'
Chagda
Ulakhan-Sulugur
Y'albyn
50km
N
Formation
Ust'-Yudoma
Pestrotsvet
Bed Number
SSF biozone
A. trisulcatus - P. anabarica
Purella antiqua
Archaeocyath biozone
D. reg.
Nm

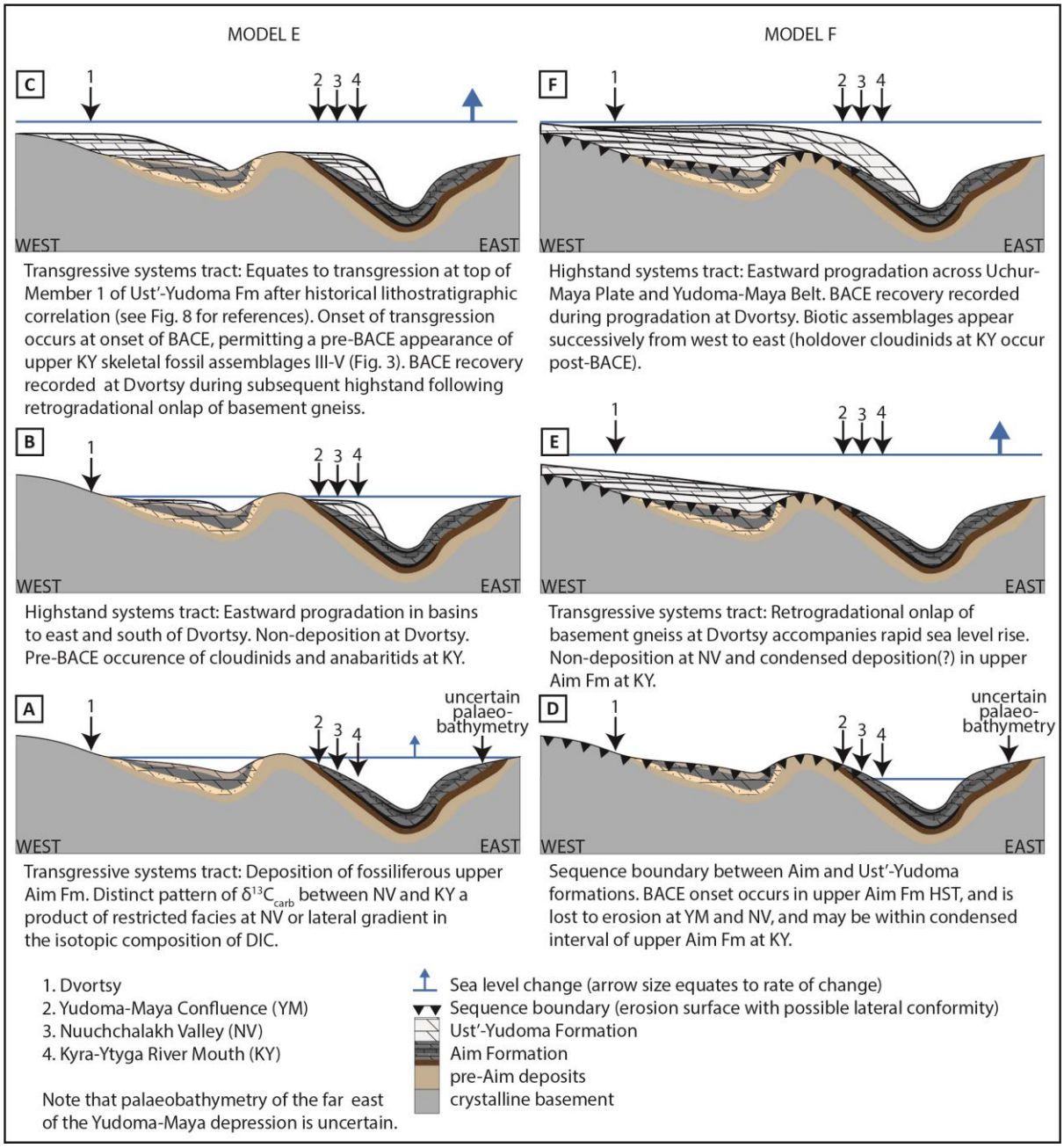
MODEL E
MODEL F
C
1
2 3 4
WEST
EAST
Transgressive systems tract: Equates to transgression at top of Member 1 of Ust'-Yudoma Fm after historical lithostratigraphic correlation (see Fig. 8 for references). Onset of transgression occurs at onset of BACE, permitting a pre-BACE appearance of upper KY skeletal fossil assemblages III-V (Fig. 3). BACE recovery recorded at Dvortsy during subsequent highstand following retrogradational onlap of basement gneiss.
F
Highstand systems tract: Eastward progradation across Uchur-Maya Plate and Yudoma-Maya Belt. BACE recovery recorded during progradation at Dvortsy. Biotic assemblages appear successively from west to east (holdover cloudinids at KY occur post-BACE).
B
Highstand systems tract: Eastward progradation in basins to east and south of Dvortsy. Non-deposition at Dvortsy. Pre-BACE occurence of cloudinids and anabaritids at KY.
E
Transgressive systems tract: Retrogradational onlap of basement gneiss at Dvortsy accompanies rapid sea level rise. Non-deposition at NV and condensed deposition(?) in upper Aim Fm at KY.
A
uncertain palaeo-bathymetry
Transgressive systems tract: Deposition of fossiliferous upper Aim Fm. Distinct pattern of $\delta^{13}C_{carb}$ between NV and KY a product of restricted facies at NV or lateral gradient in the isotopic composition of DIC.
D
Sequence boundary between Aim and Ust'-Yudoma formations. BACE onset occurs in upper Aim Fm HST, and is lost to erosion at YM and NV, and may be within condensed interval of upper Aim Fm at KY.
1. Dvortsy
2. Yudoma-Maya Confluence (YM)
3. Nuuchchalakh Valley (NV)
4. Kyra-Ytyga River Mouth (KY)
Note that palaeobathymetry of the far east of the Yudoma-Maya depression is uncertain.
Sea level change (arrow size equates to rate of change)
Sequence boundary (erosion surface with possible lateral conformity)
Ust'-Yudoma Formation
Aim Formation
pre-Aim deposits
crystalline basement

1320

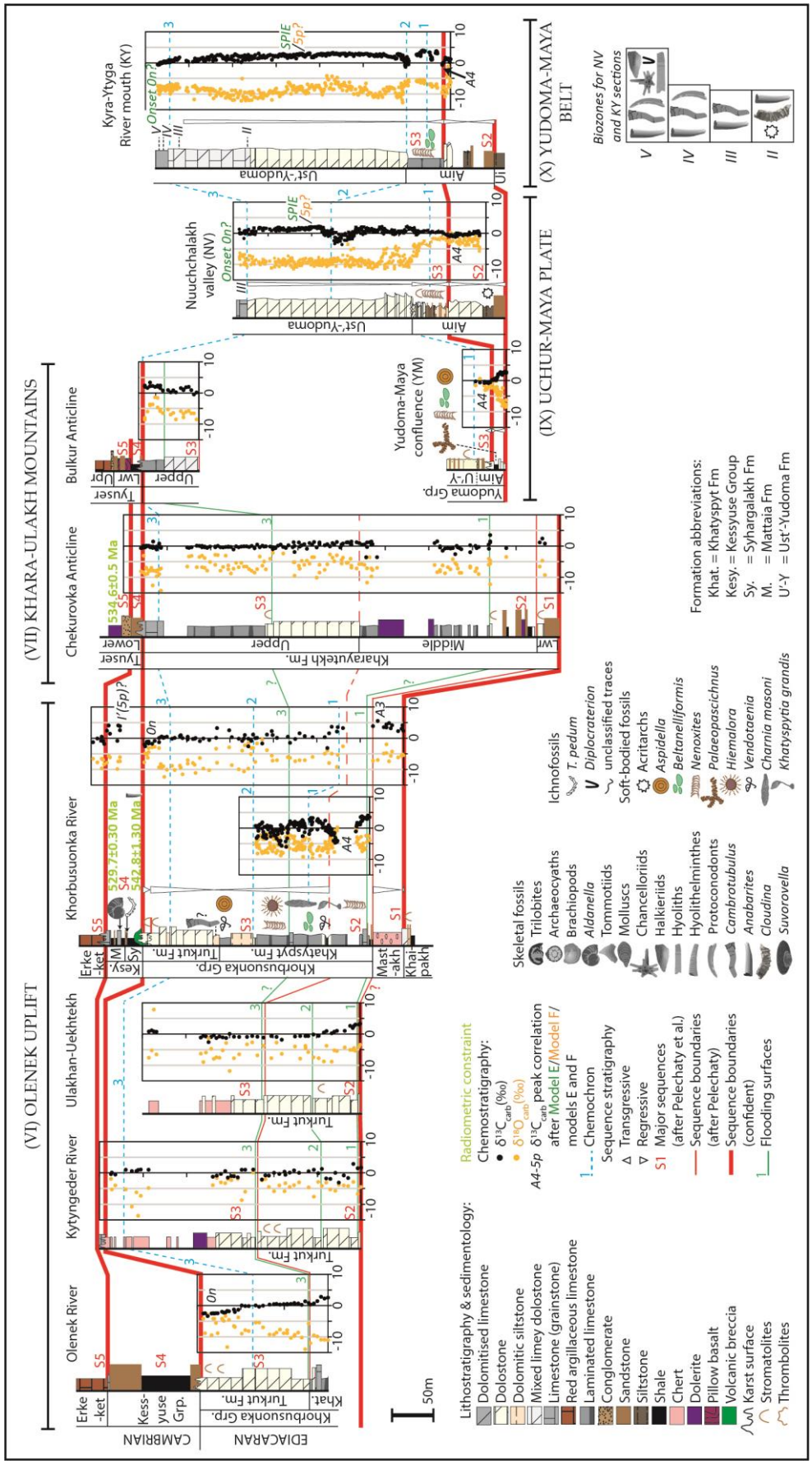
(VI) OLENEK UPLIFT
(VII) KHARA-ULAKH MOUNTAINS
(IX) UCHUR-MAYA PLATE
(X) YUDOMA-MAYA BELT
CAMBRIAN
EDIACARAN
Olenek River
Kytyngeder River
Ulakhan-Uekhtekh
Khorbusuonka River
Chekurovka Anticline
Bulkur Anticline
Kyra-Ytyga River mouth (KY)
Nuuchchalakh valley (NV)
Yudoma-Maya confluence (YM)
Onset On?
SPIE /Sp?
534.6±0.5 Ma
529.7±0.30 Ma
532.8±1.30 Ma
Lithostratigraphy & sedimentology:
Chemostratigraphy:
Skeletal fossils
Ichnofossils
Soft-bodied fossils
Biozones for NV and KY sections
Formation abbreviations:
Khat. = Khatyspyt Fm
Kesy. = Kessyuse Group
Sy. = Syhargalakh Fm
M. = Mattaia Fm
U'-Y = Ust'-Yudoma Fm
50m

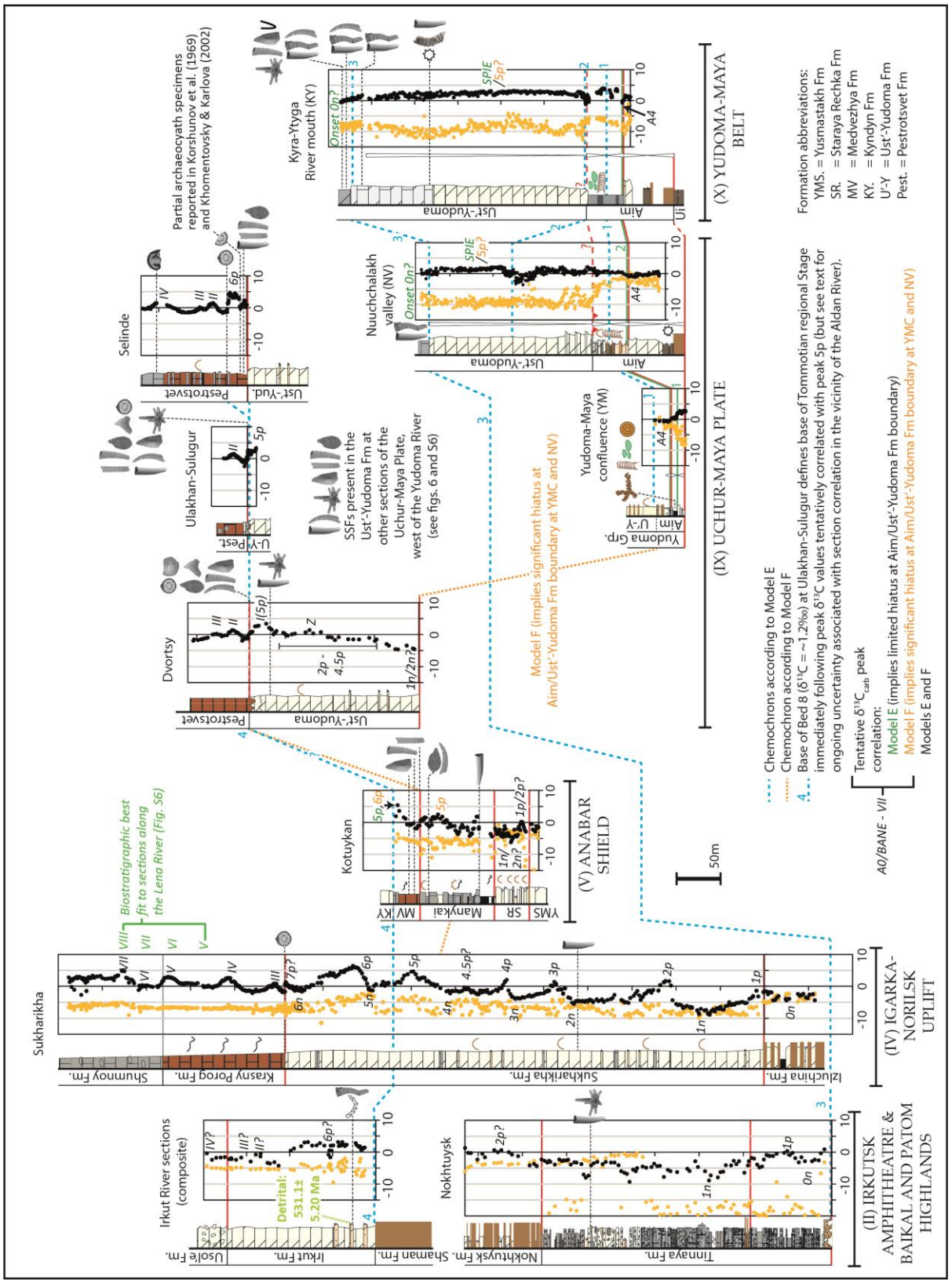
(II) IRKUTSK AMPHITHEATRE & BAIKAL AND PATOM HIGHLANDS
(IV) IGARKA-NORILSK UPLIFT
(V) ANABAR SHIELD
(IX) UCHUR-MAYA PLATE
(X) YUDOMA-MAYA BELT
Sukharikha
Irkut River sections (composite)
Nokhtuysk
Kotuykan
Dvortsy
Ulakhan-Sulugur
Selinde
Nuuchchalakh valley (NV)
Kyra-Ytyga River mouth (KY)
Yudoma-Maya confluence (YM)
Partial archaeocyath specimens reported in Korshunov et al. (1969) and Khomentovsky & Karlova (2002)
SSFs present in the Ust'-Yudoma Fm at other sections of the Uchur-Maya Plate, west of the Yudoma River (see figs. 6 and S6)
Model F (implies significant hiatus at Aim/Ust'-Yudoma Fm boundary at YMC and NV)
Biostratigraphic best fit to sections along the Lena River (Fig. S6)
Detrital: 531.1± 5.20 Ma
Chemochrons according to Model E
Chemochron according to Model F
Base of Bed 8 ($\delta^{13}C$ = ~1.2‰) at Ulakhan-Sulugur defines base of Tommotian regional Stage immediately following peak $\delta^{13}C$ values tentatively correlated with peak 5p (but see text for ongoing uncertainty associated with section correlation in the vicinity of the Aldan River).
Tentative $\delta^{13}C_{carb}$ peak correlation:
Model E (implies limited hiatus at Aim/Ust'-Yudoma Fm boundary)
Model F (implies significant hiatus at Aim/Ust'-Yudoma Fm boundary at YMC and NV)
Models E and F
Formation abbreviations:
YMS. = Yusmastakh Fm
SR. = Staraya Rechka Fm
MV = Medvezhya Fm
KY. = Kyndyn Fm
U'-Y = Ust'-Yudoma Fm
Pest. = Pestrotsvet Fm
50m

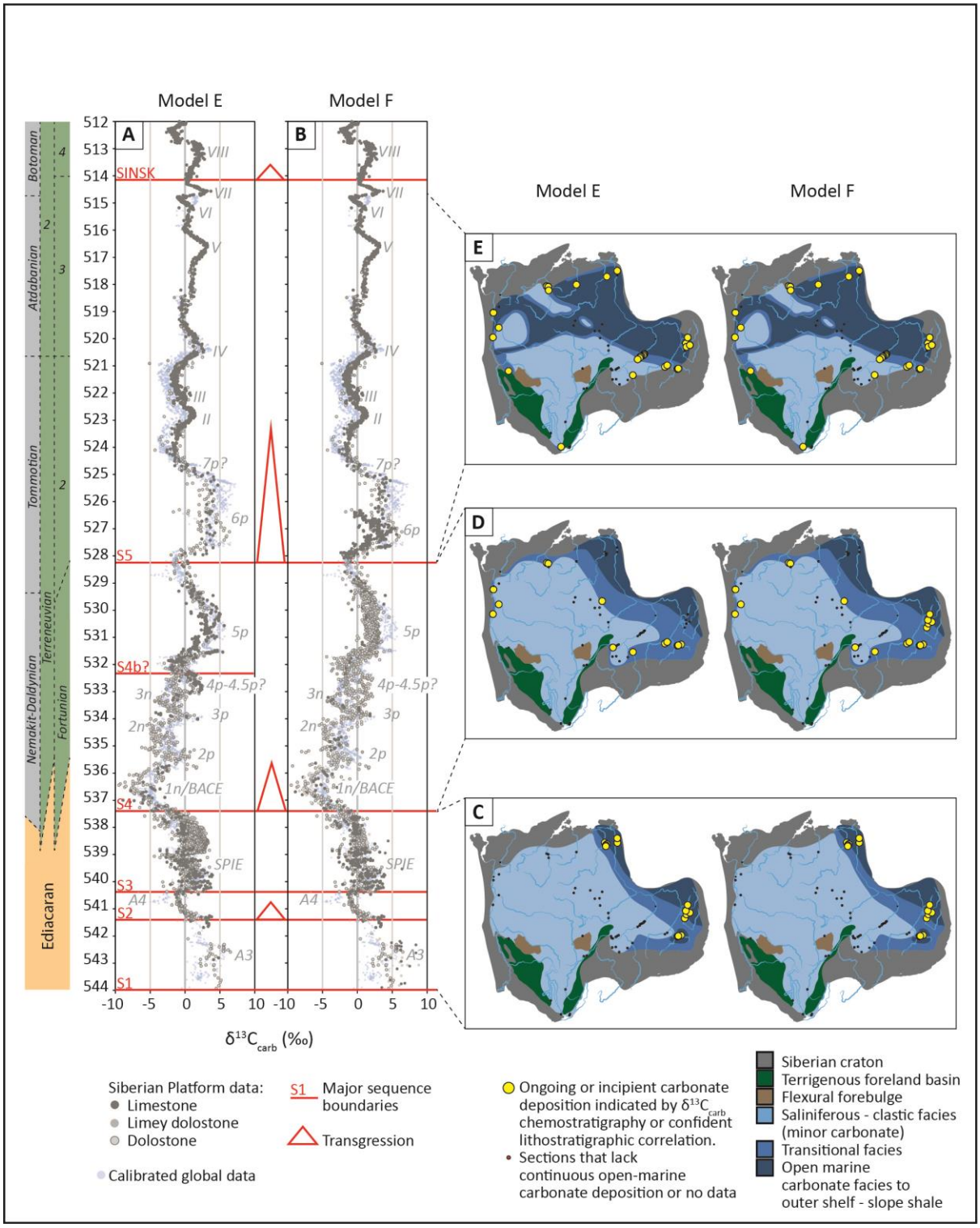
Model E
Model F
A
B
Botoman
Atdabanian
Tommotian
Terreneuvian
Fortunian
Nemakit-Daldynian
Ediacaran
SINSK
S5
S4b?
S4
S3
S2
S1
VIII
VII
VI
V
IV
III
II
7p?
6p
5p
4p-4.5p?
3n
3p
2n
2p
1n/BACE
SPIE
A4
A3
δ13Ccarb (‰)
Model E
Model F
E
D
C
Siberian Platform data:
Limestone
Limey dolostone
Dolostone
Calibrated global data
S1 Major sequence boundaries
Transgression
Ongoing or incipient carbonate deposition indicated by δ13Ccarb chemostratigraphy or confident lithostratigraphic correlation.
Sections that lack continuous open-marine carbonate deposition or no data
Siberian craton
Terrigenous foreland basin
Flexural forebulge
Saliniferous - clastic facies (minor carbonate)
Transitional facies
Open marine carbonate facies to outer shelf - slope shale

1323

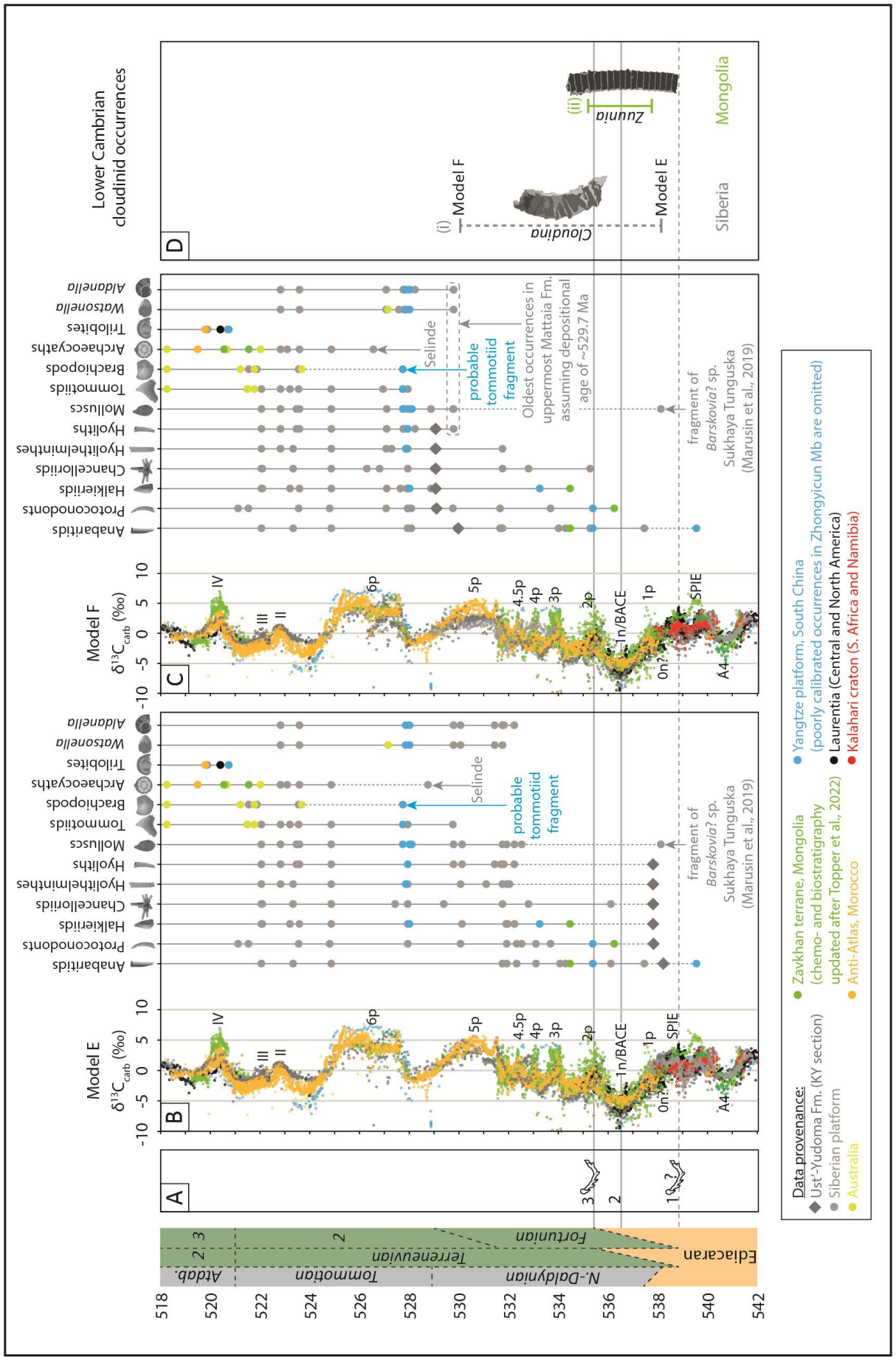
Lower Cambrian cloudinid occurrences
Model E
Model F
δ13Ccarb (‰)
Anabaritids
Protoconodonts
Halkieriids
Chancelloriids
Hyolithelminthes
Hyoliths
Molluscs
Tommotiids
Brachiopods
Archaeocyaths
Trilobites
Watsonella
Aldanella
Selinde
probable tommotiid fragment
Oldest occurrences in uppermost Mattaia Fm. assuming depositional age of ~529.7 Ma
fragment of Barskovia? sp. Sukhaya Tunguska (Marusin et al., 2019)
IV
III
II
6p
5p
4.5p
4p
3p
2p
1n/BACE
1p
0n?
SPIE
A4
Ediacaran
Fortunian
Terreneuvian
N.-Dalynian
Tommotian
Atdab.
Cloudina
Zuunia
Model F
Model E
Siberia
Mongolia
Data provenance:
Ust'-Yudoma Fm. (KY section)
Siberian platform
Australia
Zavkhan terrane, Mongolia (chemo- and biostratigraphy updated after Topper et al., 2022)
Anti-Atlas, Morocco
Yangtze platform, South China (poorly calibrated occurrences in Zhongyicun Mb are omitted)
Laurentia (Central and North America)
Kalahari craton (S. Africa and Namibia)